2018-12-01

Estimation of Knee Kinematics Using Non-Monotonic Nanocomposite High-Deflection Strain Gauges

Adin Douglas Martineau
Brigham Young University

Estimation of Knee Kinematics Using Non-Monotonic Nanocomposite High-Deflection Strain Gauges

Adin Douglas Martineau

A thesis submitted to the faculty of
Brigham Young University
in partial fulfillment of the requirements for the degree of

Master of Science

Anton E. Bowden, Chair
David T. Fullwood
Dustin A. Bruening

Department of Mechanical Engineering

Brigham Young University

ABSTRACT

Estimation of Knee Kinematics Using Non-Monotonic Nanocomposite High-Deflection Strain Gauges

Adin Douglas Martineau
Department of Mechanical Engineering, BYU
Master of Science

Human knee kinematics, especially during gait, are an important analysis tool. The current "gold standard" for kinematics measurement is a multi-camera, marker-based motion capture system with 3D position tracking. These systems are accurate but expensive and their use is limited to a confined laboratory environment. High deflection strain gauges (HDSG) are a novel class of sensors that have the potential to measure kinematics and can be inexpensive, low profile, and are not limited to measurements within a calibrated volume. However, many HDSG sensors can have a non-linear and non-monotonic response. This thesis explores using a nanocomposite HDSG sensor system for measuring knee kinematics in walking gait and overcoming the non-monotonic sensor response found in HDSGs through advanced modeling techniques.

Nanocomposite HDSG sensors were placed across the knee joint in nine subjects during walking gait at three speeds and three inclines. The piezoresistive response of the sensors was obtained by including the sensors in a simple electrical circuit and recorded using a low-cost microcontroller. The voltage response from the system was used in four models. The first two models included a physics-based log-normal model and statistical functional data analysis model that estimated continuous knee angles. The third model was a discrete linear regression model that estimated the inflection points on the knee flexion/extension cycle. Finally, a machine learning approach helped to predict subject speed and incline of the walking surface.

The models showed the sensor has the capability to provide knee kinematic data to a degree of accuracy comparable to similar kinematic sensors. The log-normal model had a 0.45 r-squared and was unsuitable as a stand-alone continuous angle predictor. After running a 10-fold cross validation the functional data analysis (FDA) model had an overall RMSE of 3.4° and could be used to predict the entire knee flexion/extension angle cycle. The discrete linear regression model predicted the inflection points on the knee kinematics graph during each gait cycle with an average RMSE of 1.92° for angle measures and 0.0332 seconds for time measures. In every estimate, the discrete linear regression model performed better than the FDA model at those points. The 10-fold cross validation of the machine learning approach using the discrete voltages could predict the categorical incline 90% of the time and the RMSE for the speed model was 0.23 MPH.

The use of a HDSG as a knee kinematics sensor was shown as a viable alternative to existing motion capture technology. In future work, it is recommended that a calibration method be developed that would allow this sensor to be used independent of a motion capture system. With these advancements, this inexpensive and low profile HDSG will advance understanding of human gait and kinematics in a more affordable and scope enhancing way.

Keywords: high deflection, nanocomposite, wearable sensor, gait analysis, kinematic sensor

ACKNOWLEDGEMENTS

This work would have been impossible without standing on the shoulders of giants. I would like to thank Dr. Bowden for teaching me optimism and for being an excellent mentor and role model. Dr. Fullwood, Dr. Seeley, Dr. Christensen, and Dr. Bruening are experts in their field and their advice greatly enhanced the quality of this work. Many thanks to Gavin Collins and Aubrey Odom who laid the foundation for the statistics of this work. Thanks to Alyssa Evans for her expertise in motion capture, exercise science, and machine learning and for being a good friend. Gratitude to my mother for teaching me courage and my father for teaching me how to work. To my wife Julieta: my editor, confidant, example, friend, and love of my life. I could not have done it without you. Finally, to the great Creator and source of all knowledge and truth; thank you for guiding me to rediscover what you already knew.

Funding was provided by the National Science Foundation under grant number CMMI-1538447. Any opinions, findings, and conclusions or recommendations expressed in this thesis are those of the author and do not necessarily reflect the views of the National Science Foundation.

TABLE OF CONTENTS

LIST OF TABLES

LIST OF FIGURES

1 INTRODUCTION

This thesis describes the implementation of a high-deflection nanocomposite strain gauge (HDSG) to measure human knee kinematics. Specifically, nickel coated carbon fiber and nickel nanostrands were mixed into a silicone matrix to create a piezoresistive strain gauge with a non-monotonic response that measured flexion-extension angles in the knee. Four models were created to estimate continuous knee flexion/extension angles in walking gait (a physics-based model and statistical based model), the inflexion points on a walking cycle, and the categorical walking incline and speed of the subject.

Chapter two presents a background literature review on knee kinematic sensors, as well as a basic introduction to gait analysis and its applications. Of note, I present a taxonomy chart of human kinematic measurement techniques, which includes the nanocomposite high deflection strain gauge sensors used in the present work.

Chapter three is the main work of this thesis. It contains the method and validation of using a non-monotonic response nanocomposite high deflection strain gauge as a kinematic sensor to measure knee angles and the speed and incline of the subject. Nine subjects walked on a treadmill at three speeds and three inclines with the HDSG and motion capture simultaneously measuring knee angles. Four different modeling techniques were used to capture distinct aspects of the subjects' knee kinematics, and the accuracy of each model was characterized. This chapter will be submitted to a peer-reviewed journal. Co-authors include: Gavin Collins, Alyssa Evans,

Aubrey Odom, Matthew K. Seeley, David T. Fullwood, William F. Christensen, Dustin Bruening, and Anton E. Bowden.

Chapter four finishes this thesis and suggests future work and direction related to this research. In particular, it points toward the integration of kinematic and kinetic sensors for a complete mobile gait analysis system.

2 BACKGROUND

2.1 Gait Analysis

Bipedal human locomotion is not only intrinsically complex but unique as a fingerprint from person to person [1]. The study of this complex locomotion or gait analysis is the investigation of the kinetics, kinematics, and muscle activation that compose human ambulation. The first recorded study of kinematics started with Aristotle and over the last two millennia of human determination and progress in technology have led to today's advancements. Through the application of Newtonian mechanics and the instrumentation of the human body through force plates, motion capture, electromyography, photogrammetry, among others, a wealth of knowledge has been created about human locomotion. This knowledge includes from the basic: the moments and forces on joints throughout healthy gait [2], to the advanced: the effects of shoe insoles on gait for those with knee osteoarthritis [3], to immediate application: diagnosis of Parkinson's disease through gait and tremor investigation [4]. Gait analysis and its tools have not only expanded understanding on how humans walk but how to use its analysis as a tool. This background will touch on lightly overall human body kinematics and focus mainly on measuring human knee kinematics with an emphasis on using high deflection strain gauges to measure knee flexion/extension angles.

The importance of gait and kinematics analysis is evident in its wide assortment of applications: cinema, biometrics, diagnosis, patient rehabilitation, and athlete performance and

improvement. In the cinematic industry, gait analysis and its tools are used to quicken the animation process by measuring human models to simulate animation characters [5]. Biometric authenticity analysts have shown that human gait is not only different from person to person but also that even poor surveillance video can be used to correctly identify individuals [1]. Evidence for gait analysis as a diagnostic tool spans many diseases: Alzheimer's [6], Parkinson's [7], rheumatoid arthritis [8], cerebral palsy [9, 10], muscular dystrophy [11], and multiple sclerosis [12]. Some researchers have taken it a step further and used gait analysis as a rehabilitation tool to quantify the recovery of total knee replacements [13]. On the opposite end of the spectrum, motion capture analysis has also been used to increase athlete performance such as increasing jump height in volley ball players [14]. Motion capture has also been used to provide evidence for changing gymnastic technique on the uneven bars [15]. The influence of motion capture in athletics extends to equipment optimization [16]. These applications exemplify how ubiquitous gait and kinematic analysis has become and its importance as a tool.

2.2 Measuring Gait Kinematics

Since the application of gait analysis varies widely and spans multiple industries the tools that measure kinematics also vary widely. The tools can be broadly separated into two groups (Figure 2-1). First, tools that use a calibrated volume and are subsequently volume restrictive. These include video motion capture through normal video cameras and physical rods that specify calibrated distances, X-ray motion capture through fluoroscopy and sometimes markers, and infrared (IR) motion capture through markers and IR cameras. Another group can be broadly categorized as body mounted sensors that include goniometers, inertial measurement units (IMU), exoskeletons, and high deflection strain gauges directly attached to the body. All these techniques offer ways to measure kinematics and gait of the human body.

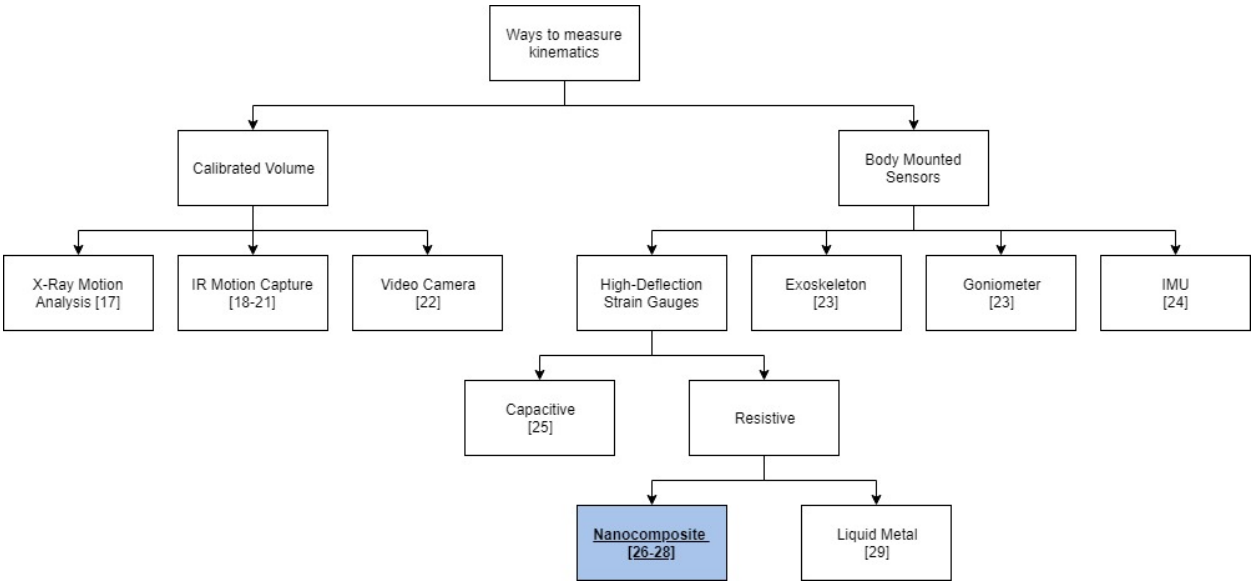

Figure 2-1: Measuring space for quantifying human knee kinematics. This paper's sensor space is highlighted in blue.

Calibrated volume techniques provide high accuracy with tradeoffs in types of activities that can be measured. IR motion capture is the "gold standard" and is the basis to which most kinematic systems are compared to. It uses markers that reflect infrared light back to specialized cameras and with marker position can have an accuracy of 63±5 μm and a precision of 15 μm when measuring rigid bodies [21]. In terms of rigid bodies angles, Maletsky et. al. reported that at 10° rotation bias was 0.05° and a 95% repeatability limit of 0.67° [19]. Though these errors are miniscule when measuring rigid hinge joints, the error from motion capture calculated human knee joint angles increased because of soft tissue artifacts and errors associated with assuming the knee is a revolute or spherical joint. One way soft tissue artifacts have been quantified is through comparing markers attached to the skin and markers attached directly to the bone through pins. When compared to intra-cortical bone pins the rotational soft tissue artifact RMSE measured was 2.1° [30]. Andersen et. al. also conducted a study using a similar method and found the mean error estimates in flexion/extension angles increased 0.6°±0.6° by using a

spherical joint model and 1.0°±1.2° for a revolute joint model [31]. When comparing other kinematic measurement methods to this "gold standard", it is important to consider the aggregate error that stems from soft tissue artifact and modeling limitations are reasonably within 1°-2°. With these relatively small errors, cost for IR motion capture varies widely but can reach in the millions for buying the cameras, markers, software, and for maintenance of the system.

X-ray motion capture is also very accurate with less than 10 μm accuracy and a precision of 46 μm when measuring rigid bodies [17]. Fluoroscopy, as it is also known, has the advantage of visualizing the bone directly for calculation of angles. Standard video cameras can be used to measure three-dimensional information by using calibration rods with known distances and at least two cameras. Two dimensions can also be measured by using one camera and similar calibration rods. Accuracy of 2-D video cameras measuring body angles are more accurate in the sagittal plane than the frontal plane when compared to a 3-D motion capture system [22]. Specifically, the trunk, hip, knee, and ankle sagittal angles and knee frontal angles from 2-D video cameras were statistically equivalent to a 3-D IR motion capture system [22]. All these methods are only possible within a pre-calibrated volume which eliminates the ability to measure quotidian life.

Goniometers, exoskeletons, inertial measurement units (IMU), ultrasound, and radio are body mountable kinematic sensors that can be used to measure joint angles (Figure 2-1). Goniometers come in both digital and analog varieties. The digital kind have an accuracy of less than 2° at each joint, requires precise alignment at each joint, and can limit the subject's range of motion [23]. The digital goniometer's power consumption is low [23]. Exoskeletons are full body suits that use potentiometers, encoders, or goniometers to measure body angles and, in many cases, offer mechanical support for the user [23]. They also have less than 2° accuracy at

each joint [23]. Yet, they require several batteries to function for just a few hours but are excellent for rehabilitation applications [23]. IMUs which are composed of an accelerometer, gyroscope, and magnetometer have an accuracy of less than 2° at each joint but can be affected by external interference and measurement drift [23, 24]. Their low power consumption makes them available to collect data anywhere from 1 day to 1 week [23]. Ultrasound, short-range radio, ultra-wideband, and radio frequency identification have been used in conjunction with IMUs to add additional location information to reduce signal drift in IMUs effectively [23, 25, 32]. Many body-mounted sensor systems have built a strong foundation for mobile gait analysis techniques.

2.3 Measuring Knee Kinematics Through a High Deflection Strain Gauge

High deflection strain gauges (HDSG) come in many forms but can be divided into two main groups: capacitive and resistive (Figure 2-1). Capacitive strain gauges in general have two conductive films separated by an insulative layer whose thickness changes as they are strained. This in turn changes the capacitance between the two layers [25, 32]. Nakamoto et. al. used a capacitive strain sensor to measure knee and ankle flexion/extension angles compared to motion capture in one healthy male subject [25]. For knee flexion/extension angles, the subject flexed his knee at interval chimes played at 0.67 Hz while measuring the sensor voltage and motion capture angles. Overall the mean error was 4.4° over a complete cycle but decreased to 1.7° for the knee in extension and increased to 8.9° while the knee was in flexion.

More studies have shown evidence that resistive type strain sensors have the ability to measure human knee kinematics [26, 27, 29]. These resistive strain gauges can be divided into two groups: nanocomposites and liquid metal films (Figure 2-1). Nanocomposite HDSG consist

of a conductive particle or strand suspended in a flexible matrix. Cheng et. al. demonstrated the capabilities of their novel sensor, a graphene-based fiber in polyurethane, by measuring the knee during flexion and extension, walking, jogging, jumping, and squatting [26]. They did not however, compare the sensor values to motion capture or any other sensor. Yamada et. al. also measured the knee with a carbon nanotube film strain gauge during multiple activities including extending, flexing, marching, squatting, jumping, and jumping from squatting but also without comparison to motion capture [27]. Mengüç et. al. used a liquid metal high deflection strain gauge to measure hip, ankle, and knee kinematics during walking and running gait with moderate accuracy [29]. Specifically, the RMSE for knee flexion extension angles was at best close to 4° for 2 MPH walking and at worst 15° for 6 MPH running [29]. High deflection resistive strain gauges have the potential to measure knee kinematics accurately in human gait.

2.4 Nickel Coated Carbon Fiber and Nickel Nanostrand High Deflection Strain Gauge

The HDSG of this thesis is a piezoresistive nanocomposite sensor made up of nickel nanostrands (NINS) and nickel coated carbon fiber (NCCF) in a silicone matrix. The piezo resistivity of this sensor is thought to be caused by two major phenomena: quantum tunneling and percolation theory [33-35]. As the sensor is strained, the distance between the conductive particles in the insular matrix changes. The distance, or gap size, is directly proportional to the probability that an electron will jump or quantum tunnel from one conductive particle to the next. The minimum distance an electron will tunnel from one conductive particle to the next is the barrier height. Percolation theory states that the electrons will subsequently follow the random array of conductive particles and gaps smaller than the barrier height until they have gone from one end of the sensor to the other. The overall resistance decreases in the sensor as the size of the gaps decrease. This creates a non-monotonic log-normal response described by Baradoy and

Johnson (Figure 2-2) [36, 37]. Baradoy specifically found that the slopes of region 1 and 2 and the critical strain (the strain where region 1 and 2 meet) of this log-normal curve could be characterized by the percent volume fractions of NINS and NCCF added [36]. This allows the strain gauge to be customized according to the needs of the application. For example, high slopes of regions 1 and 2 would turn the sensor into a switch at a specific strain. In contrast, a lower slope allows a larger region where the sensor can measure a more gradual change in strain. The physics behind the HDSG lend itself to be used in a high-strain sensing application.

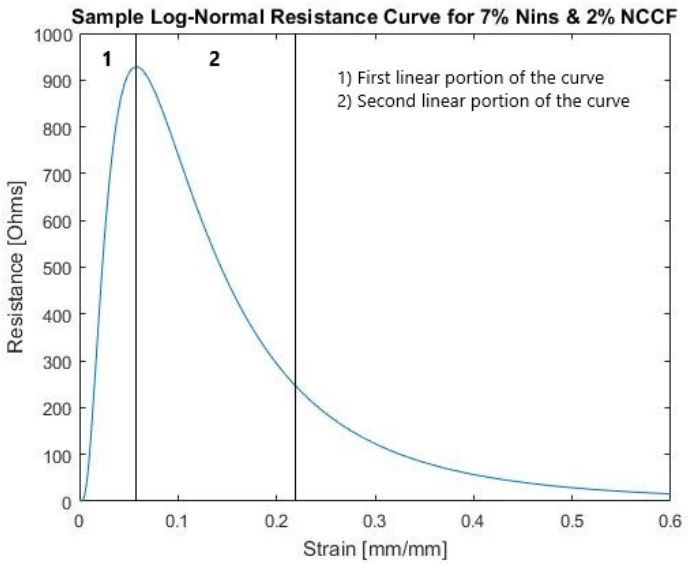

Figure 2-2: Sample log-normal response of a high deflection nanocomposite strain gauge.

The same physics that allow the sensor to be customable also creates a non-monotonic strain response. In previous work the HDSG has accurately predicted sitting posture [38], measured contractions during pregnancy [36], and measured ligament strain [39]. In general, these applications applied a pre-strain to avoid the first linear region of the log-normal curve and avoid difficulties of modeling the non-monotonic nature of the piezoresistive response. This

thesis explores simplifying the implementation of the nanocomposite, non-monotonic, HDSG by modeling the sensor while it is being utilized in regions 1 and 2 of the strain resistance response during human walking gait.

The high deflection nanocomposite strain gauge's modulus and strain at break allow it to be used in human measurement applications. The modulus must closely match the item being measured in order not to change the kinematics of the system. A higher strain at break allows the sensor to measure at larger strains before breaking. There are two main types of matrices used so far in HDSG nanocomposites: Sylgard and Ecoflex. With Syglard as the matrix the modulus was a high 1.84 MPa and a strain at break of 40% [40]. Ecoflex performs a bit better especially for human skin strain applications. Its modulus is much closer to skin with 0.37 MPa and a strain at break of 50-80% [41]. For a human knee angle kinematic application, Ecoflex is best suited because of its higher strain at break and modulus closer to the modulus of human skin [32].

3 ESTIMATING WALKING HUMAN GAIT KNEE KINEMATICS WITH NANOCOMPOSITE HIGH DEFLECTION STRAIN GAUGES

3.1 Abstract

This paper describes a method to measure knee kinematics using a nanocomposite high deflection strain gauge (HDSG) sensor system with a non-monotonic sensor response during walking gait. Nine subjects (6 males, 3 females) walked on a treadmill at three speeds and inclines with a HDSG over the right knee. Voltage from the HDSG, was used in four models to estimate knee angles, measured by the motion capture IR cameras, and speed and incline, designated by an instrumented treadmill. First, a physics based, log-normal model computed continuous knee angles with an r-squared of 0.45. Second, a functional data analysis approach found through a 10-fold cross validation process estimated continuous knee angles with an overall RMSE of 3.4°. Third, a discrete linear regression model estimated the inflection points on the knee flexion/extension cycle with an average RMSE of 1.92° for angle measures and 0.0332 seconds for time measures. Finally, a machine learning approach went through a 10-fold cross validation and predicted subject speed with an RMSE of 0.23 MPH and predicted categorical incline (3% incline, level, or 3% decline) 90% of the time. Through advanced modeling techniques, the HDSG sensor system could accurately estimate knee flexion/extension angles outside of a traditional laboratory setting despite its non-monotonic sensor response.

3.2 Introduction

Bipedal locomotion is a feat of nature and has been studied formally since Aristotle. Modern multi-camera video motion capture systems record the movements of locomotion accurately at high spatial resolution, but carry a high monetary cost from the perspectives of hardware, software, and data analysis time [10], and are limited to a confined laboratory environment [23]. Increased availability of accurate locomotion measurement through the introduction of a sensor system that is inexpensive, wearable, and unconstrained by calibrated volumes could dramatically increase both the availability and potential applications of locomotion analysis. In particular, high-deflection strain gauges (HDSG) represent a novel class of sensors that holds potential to fill this void. Though resistive HDSG sensors can have a high gauge factor [32, 34, 42-48], their non-linear properties [27, 32, 37, 42, 45, 47, 49-52] can make them difficult to use as a sensor. This paper seeks to develop techniques to use a non-monotonic HDSG as a wearable sensor to measure knee kinematics.

Over the last decade, the types of sensors used to measure human kinematics has greatly expanded, thus it makes sense to give context to the HDSG sensors used in this work in the context of a taxonomy chart (Figure 2-1). As noted in the chart, they can be classified as body-mounted sensors which operate by measuring wide-range strains using changes in the electrical resistance of the sensor. Advantages of a HDSG approach include flexibility in spatial location of the activity being measured (lack of a need to operate in a calibrated volumetric space) [25, 29, 32], low-profile, non-intrusive sensor mounting, and in many cases (including this work), low cost (e.g. the materials cost for the HDSG sensor cost was 2.06 USD). Disadvantages include material creep (the matrix material of these sensors is typically an elastomeric polymer) [32, 53], electrical signal drift (due to electromechanical degradation of connectivity of the

network of conductive nanofillers) [53], sensitivity of the sensor properties to ambient conditions (i.e. temperature) [32], and a nonlinear strain-resistance response [32, 37, 47].

Recent work in developing HDSGs has indicated that they may be an excellent choice for measuring human kinematics. As noted in Figure 2-1, high-deflection strain gauges can be broadly divided into two categories: resistive and capacitive. Resistive type gauges are more common when it comes to measuring human movement. The activities they have been used to measure range from large deflection activities like a squat jump to minute deflection changes like breathing [23, 27], and include measuring motion of human fingers, throat, forearm, elbow, hip, ankle, and knee [27, 29, 42, 54-56]. Linearly modeled HDSGs have shown they have the potential to measure articular motion, however many high-deflection strain gauges exhibit a more complex, non-linear electromechanical response and require more advanced modeling techniques [32, 37, 42, 45, 47, 49-52].

The present work utilized a specific HDSG sensor, which was invented at Brigham Young University and is comprised of nickel nanostrands (NiNs) and nickel coated carbon fiber (NCCF), which are sparsely dispersed throughout a silicone matrix. These conductive fillers create a piezoresistive effect through a combination of quantum tunneling and percolation theory [34]. The sensors exhibit a characteristic log-normal piezoresistive response (Figure 2-2). The slopes of regions 1 and 2, as well as the critical strain (i.e., the inflection point separating regions 1 and 2 in Figure 2-2), of this HDSG can be tailored according to the desired sensor characteristics for a particular application. For example, some applications may require a narrow piezoresistive response curve that acts as a "switch" at a specific strain, while others, such as kinematic analysis, benefit from a more graded response over a broad strain range. Tailoring of the piezoresistive response is accomplished through variation of the volume percentage of each

conductive filler element (NiNs, NCCF) added to the matrix [36, 37]. In previous work, this HDSG has been used to accurately predict sitting posture [38], measure maternal contractions during pregnancy [36], and measure ligament strain [39]. Typically, these applications have leveraged the 2nd linear region of the piezoresistive response (region 2 of Figure 2-2), by applying a pre-strain to the sensor to avoid the difficulties of modeling the non-monotonic nature of the piezoresistive response. This paper explores using this sensor in the non-monotonic region (Region 1 & 2 of Figure 2-2) of the strain resistance response, which facilitates a simpler implementation, but requires a more challenging sensor model. It also validates the wearable HDSG sensor system measuring one degree of freedom knee flexion-extension angles during walking gait.

3.3 Methods

HDSG sensors were made using Ecoflex 00-30 two-part platinum-catalyzed silicone, 9% by volume nickel nanostrands (Conductive Composites, UT, USA), and 3% by volume nickel coated carbon fiber (1 mm chopped 20% Ni) (Conductive Composites, UT, USA). This mixture was placed into the 50.6mm x 101.45mm x 1mm female portion of the aluminum mold shown in Figure 3-1 and placed in a vacuum at -20Pa for 5 min. The mixture was smoothed out and the male portion was placed into female portion, secured with c-clamps and cured at room temperature for twenty-four hours. The gauge was then removed and cut into 6mm x 1mm x 101.45mm strips. The strips were cyclically strained to 50% strain on a materials testing machine (Instron®, MA, USA) until <1% permanent deformation strain change between cycles was observed (approximately 5 cycles). This preconditioned sensor was placed in a metal crimp on each end that connected to the electric circuit (Figure 3-2). The metal crimp connectors were

glued to athletic tape (KT Tape®, UT, USA) and the entire construct was covered with an insulating layer of silicone glue (Sil-Poxy©, Smooth-On Inc., PA, USA). This sensor was then placed in a voltage divider circuit which was connected to and compared with ground (Figure 3-2). The voltage supplying this circuit was a 3.2 V AC, 100 Hz square wave. A 1.66 Kohm resistor was the other element in the circuit. A custom microcontroller collected the voltage data at 1031 Hz specified by the timer in the microcontroller (Figure 3-2). The voltage data was down-sampled to 1000 Hz and the root mean square average of each complete square wave cycle (10 points) was computed, allowing for an exact match to the sampling frequency of the motion capture data.

Figure 3-1: Mold for HDSG.

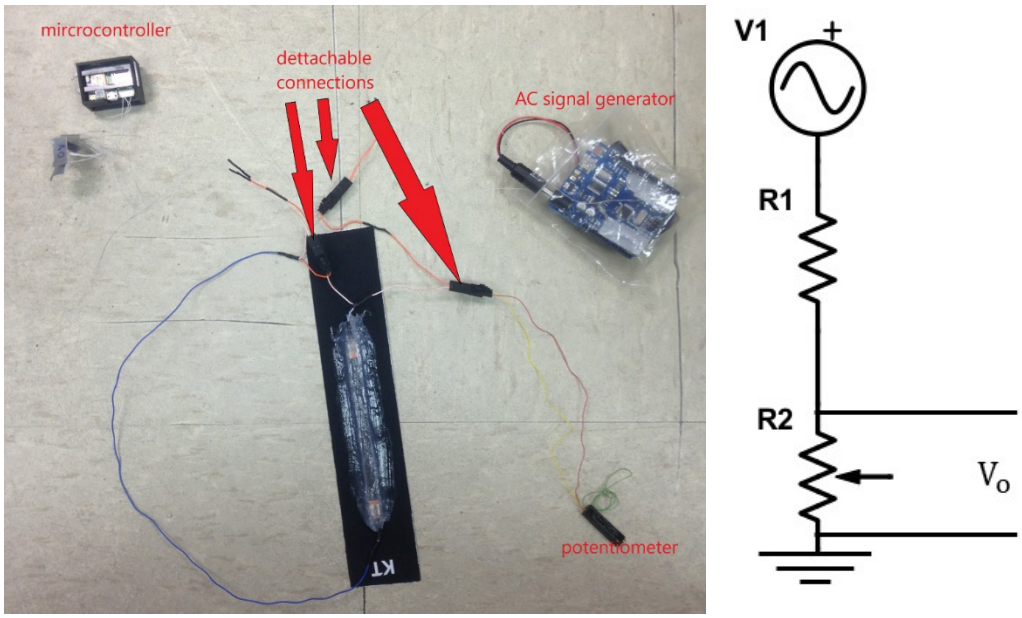

Figure 3-2: HDSG connected to voltage divider and circuit schematic. R1 = fixed resistor, R2 = HDSG, and V1 =AC source.

The HDSG sensors were utilized to capture a suite of 9 separate trials conducted on 10 individual subjects (90 total trials). Subject gender was mixed (4 females and 6 males) and ages ranged from 52-60 years old (mean 55.4 y.o.) (age was selected based on potential applications with Alzheimer's, knee osteoarthritis, and total knee replacement). Each subject had the HDSG sensor and circuit placed on their right knee approximately over the patella (Figure 3-3). One cluster of reflective markers was placed on the shank and another on the thigh. Subjects were instructed to straighten legs during the static trial. This data was compared to motion capture (Vicon Motion Systems, United Kingdom) data collected at 100 Hz which was processed through Visual 3D (C-Motion Inc., MD, USA) to get flexion and extension knee angles through the native knee model found in Visual 3-D. Subjects completed 9 trials each: 3 walking speeds (slow, medium, fast) at 3 distinct inclines (level, 3% uphill, or 3% downhill). Before data collection, subjects were instructed to walk on the treadmill and notify the data collector what

treadmill speed they felt comfortable walking while the data collector increased the speed in 0.5 MPH increments. All subjects selected 2 MPH as the slow walk, medium walk was either 2.5 or 3 MPH, and fast walk was either 3.5 or 4 MPH. Trials were excluded if missing marker data made it impossible to extract motion capture data and a treadmill malfunction prevented acquisition of downhill data for one subject. One subject was completely excluded because an improper static trial made it impossible to extract motion capture data. After data exclusion, there were 61 complete trials included in the study from 9 subjects.

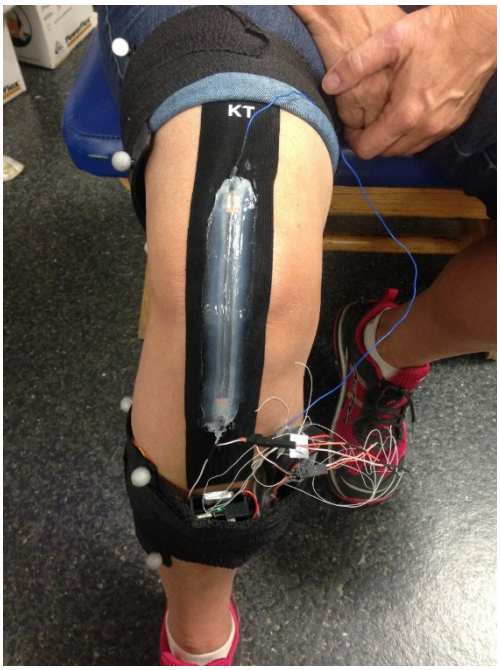

Figure 3-3: HDSG set up applied to a subject.

Data from the HDSG were analyzed using four separate models: a modified log-normal model (Matlab, Mathworks, MA, USA), functional data analysis model (FDA) (R Software), discrete linear regression model (R Software), and a machine learning speed and incline model

(WEKA, University of Waikato, New Zealand). Depending on the application, different modeling techniques are needed to provide the appropriate accuracy in the measurement and the necessary information for that application. There are four main users of kinematic human data: biomechanists, exercise scientists, physicians, and athletes. In biomechanical research, continuous knee flexion/extension data is needed to calculate power and joint moments. Currently, infrared motion capture techniques have an RMSE close to 2° on the knee when compared to bone pins [30, 31] If continuous knee angle estimation is close to this error it could be deemed acceptable to biomechanists. A simple physics-based model based on the natural phenomena of the sensor is best suited for continuous knee angle estimation if the accuracy is high. The modified log-normal model fits this category (Figure 3-4) and was based on a previously reported quasi-static relationship between the sensor strain and sensor resistance (e.g., Baradoy [36]). If the accuracy is not high enough in the physics-based model, a statistical approach that is dependent on the application can be used to achieve higher accuracy. The FDA model utilizes this statistical approach and was used to estimate continuous knee angles throughout the gait cycle (Figure 3-4). Physicians and at times exercise scientists only need specific points on the knee walking gait cycle with high fidelity. The accuracy needed for discrete measures is dependent on the application. In general, differences between control and pathological groups were found using motion capture. If the discrete model RMSE is also comparable to motion capture error, it could be used as an acceptable tool to exercise scientists and physicians. The discrete linear regression model was used to estimate inflection points on the knee flexion/extension gait cycle with high fidelity (Figure 3-4). Finally, general information like speed and slope of the incline are useful for athletes and exercise scientists for performance measurement. Currently athletes use IMUs to measure speed and incline and if HDSG match

their RMSE error HDSG could be used as a suitable replacement. The machine learning models helped to quantify this performance (Figure 3-4) and were used to estimate the speed and slope of the trial (necessary prerequisites for accurate models of caloric expenditure [57, 58]). More detailed information on the specific implementation of each model is provided in the corresponding results section below.

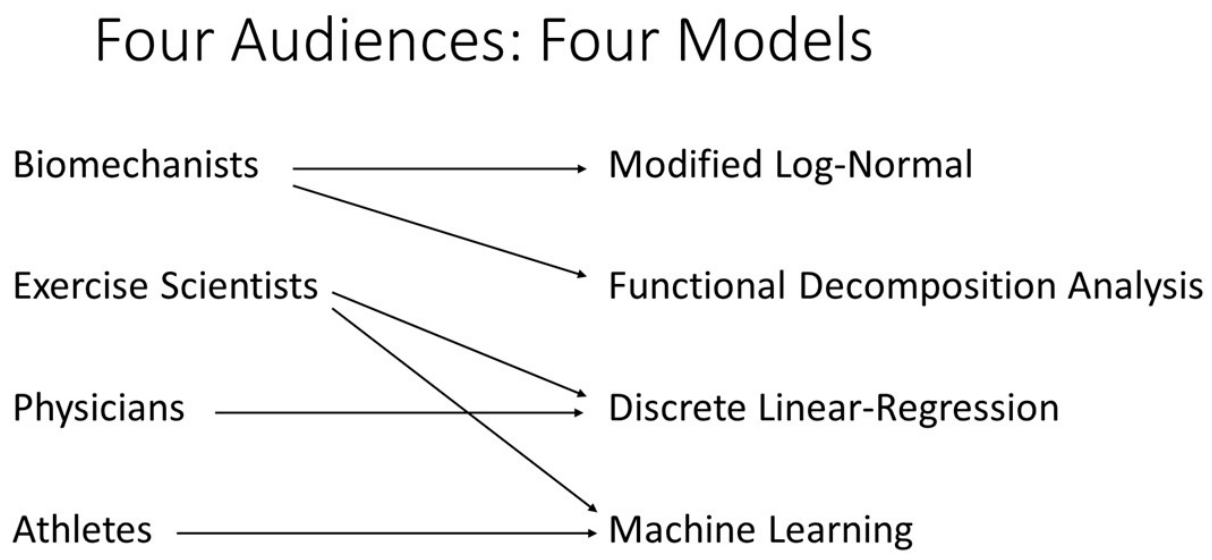

Figure 3-4 Audiences for each kind of model.

3.4 Results

3.4.1 Modified log-normal model

The nonlinear log-normal model was a curve-fit parametric model based on the underlying sensor physics but does not consider time-dependent phenomena. This modified log-normal model was fit to all the trials within each subject (3-1) taken from a previous log-normal

characterization of a similar gauge by Baradoy [36]. Knee angle was used as the independent variable and the voltage as the dependent variable to make the model a one-to-one function. A non-linear least squares optimization routine was used to identify three model-characteristic parameters: *a* (the shape parameter), *c* (x-axis scaling parameter), and *d* (y-axis scaling parameter). Bi-square weighting was the parameter that was minimized. The r-squared was extracted to determine how much the instantaneous sensor signal in isolation could predict knee angles without requiring a more complex model.

$$\text{Voltage} = \mathrm{d}\left[\frac{1}{\mathrm{a}\left(\frac{\mathrm{x}+\mathrm{x0}}{\mathrm{c}}\right)\sqrt{2\pi}}\mathrm{e}^{\left(-\frac{\ln\left(\frac{\mathrm{x}+\mathrm{x0}}{\mathrm{c}}\right)^{2}}{2\mathrm{a}^{2}}\right)}\right] \tag{3-1}$$

The r-squared for all subjects was 0.45 for the models. The data distribution around the model was very spread (Figure 3-5). The sensor voltage dependency upon knee angle generally followed the modified log-normal function, but overall curve shape was not as steep in region two as previously reported by Baradoy. This is likely a consequence of a different sensor formulation combined with the fact that knee angle is not a linear surrogate for strain. Baradoy also reported only single cycle to failure testing of the piezoresistive response, thus his models failed to capture the hysteresis inherent in the sensor system.

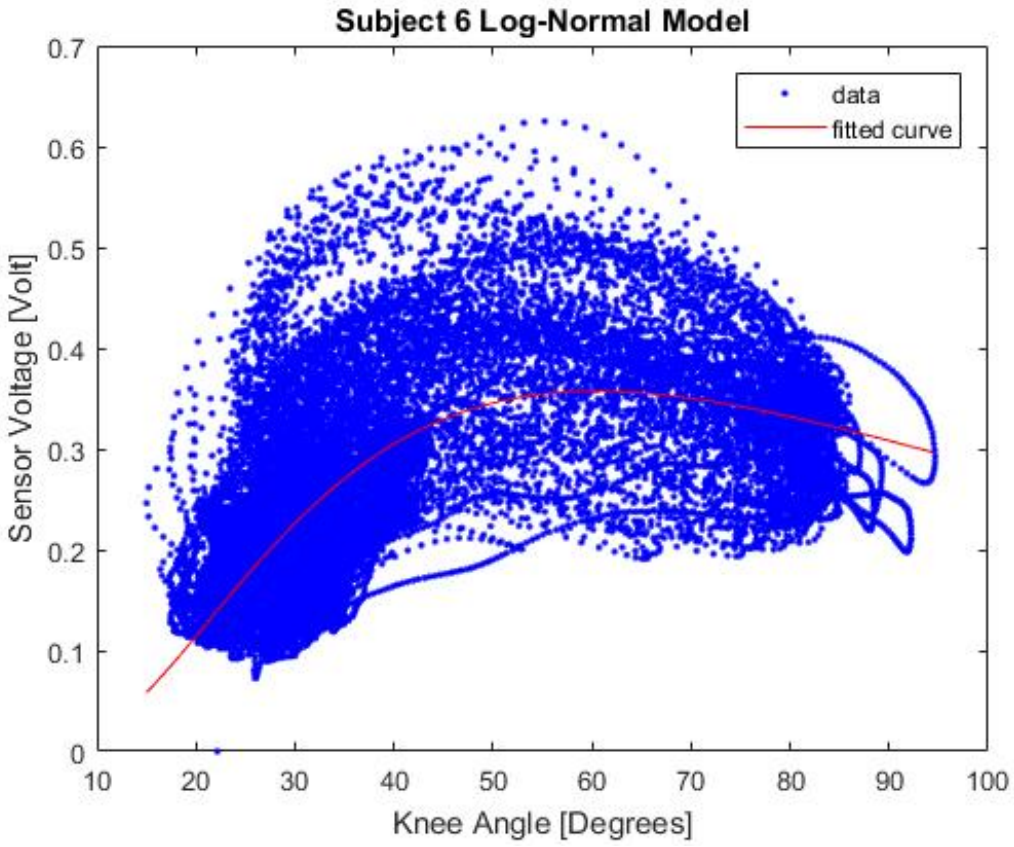

Figure 3-5: Example of log-normal fit for subject 6.

3.4.2 Functional data analysis model

The FDA model was used to estimate continuous knee angles throughout the entire stride (useful for calculating joint power and moment for orthopedic applications). Knee angle and voltage data were separated into strides manually, where the beginning of each stride was identified as the time at which a relative minimum occurred in the knee angle data, just prior to the peak angle of the stance phase. Knee angle and voltage data were resampled to 100 data points per stride to facilitate the functional data of the stride for statistical analysis, and the derivative of the voltage data was computed at each point. Each stride of the knee angle data, the

voltage data, and derivative of voltage data was then assigned a smooth representation using a 17-term Fourier series (an intercept, 8 sine, and 8 cosine terms) for use in a functional linear model (3-2). Because of essential characteristics of the voltage data between subjects, a separate model was built for each of the nine subjects. This would require a calibration procedure for each subject in a practical setting. For subject $\mathrm{j} = 1, \ldots, 9$, let $\theta_i(t)$ be the Fourier representation of the subject's i_{th} knee angle stance, $\mathrm{i} = 1, \ldots, \mathrm{n_j}$, where n_j is the total number of stances for subject *j*. We model $\theta_i(t)$ as follows:

$$\theta_i(t) = \beta_0(t) + v_i(t)\beta_v(t) + d_i(t)\beta_d(t) + \varepsilon_i(t) \qquad (3\text{-}2)$$

where $\theta_i(t)$, $v_i(t)$, and $d_i(t)$ are the Fourier representations of the subject's i_{th} knee angle, voltage, and derivative of voltage strides, respectively, at time $\mathrm{t} \in 1 \ldots 100$. The function $\beta_0(t)$ is the intercept term and is a very close imitation of the subject's mean knee angle curve. The terms $\beta_v(t)$ and $\beta_d(t)$ are functional coefficients associated with the voltage and the derivative of voltage data, respectively. These coefficients are optimized to leverage correlation between the voltage and knee angle data in order to pinpoint stride-to-stride differences in the subject's knee angle. Finally, $\varepsilon_i(t)$ represents the residual error term for stride *i* at time *t*. For the details of fitting a functional linear model, see Ramsay et. al. [59].

Figure 3-6 shows both the measured angle and the predicted angle from a representative stride for that subject. The model performed moderately well in predicting individual stances, but we noted that it performed exceptionally well at predicting the average stance of each subject (Figure 3-7). This performance at predicting the average continues across all speeds and inclines

(Figure 3-8). Table 3-1 details the performance of the functional data model at each speed and incline. The model's RMSE seems to be more consistent across inclines than across speeds. Using a 10-fold cross validation, the continuous functional data models on average had an RMSE of 3.4° for all subjects across all trials. By stance, the highest error occurred at the transition from stance phase to swing phase (Figure 3-9).

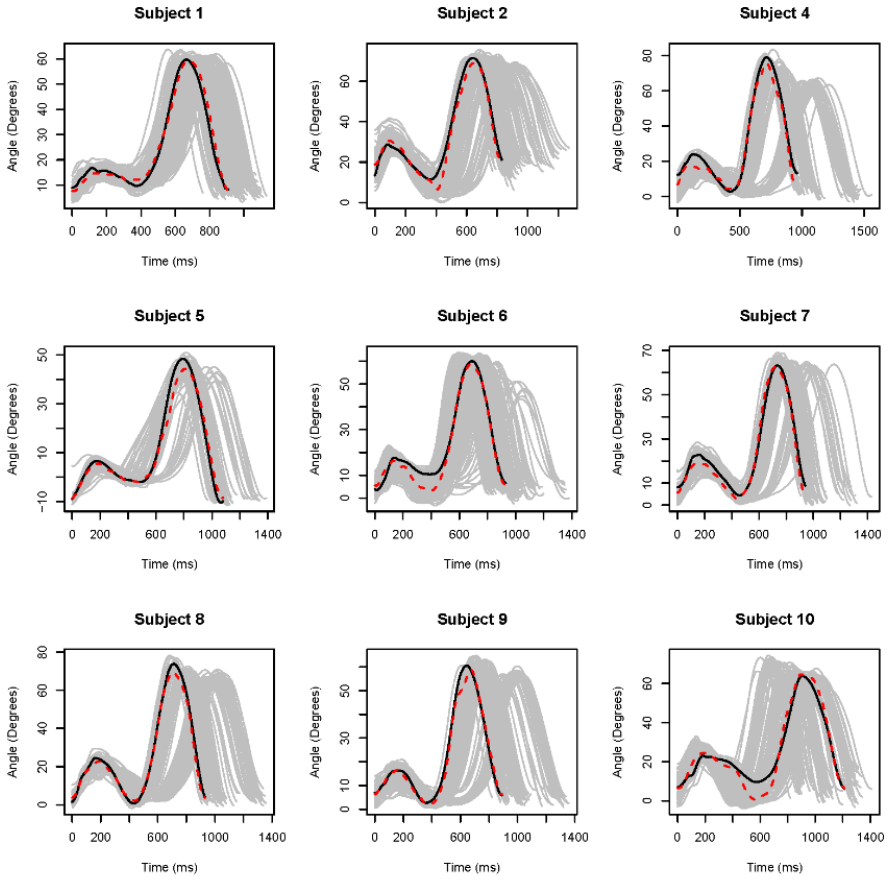

Figure 3-6: All stances for all subjects depicted in gray. The stance with the lowest RMSE prediction in dotted red and the corresponding angle depicted in black.

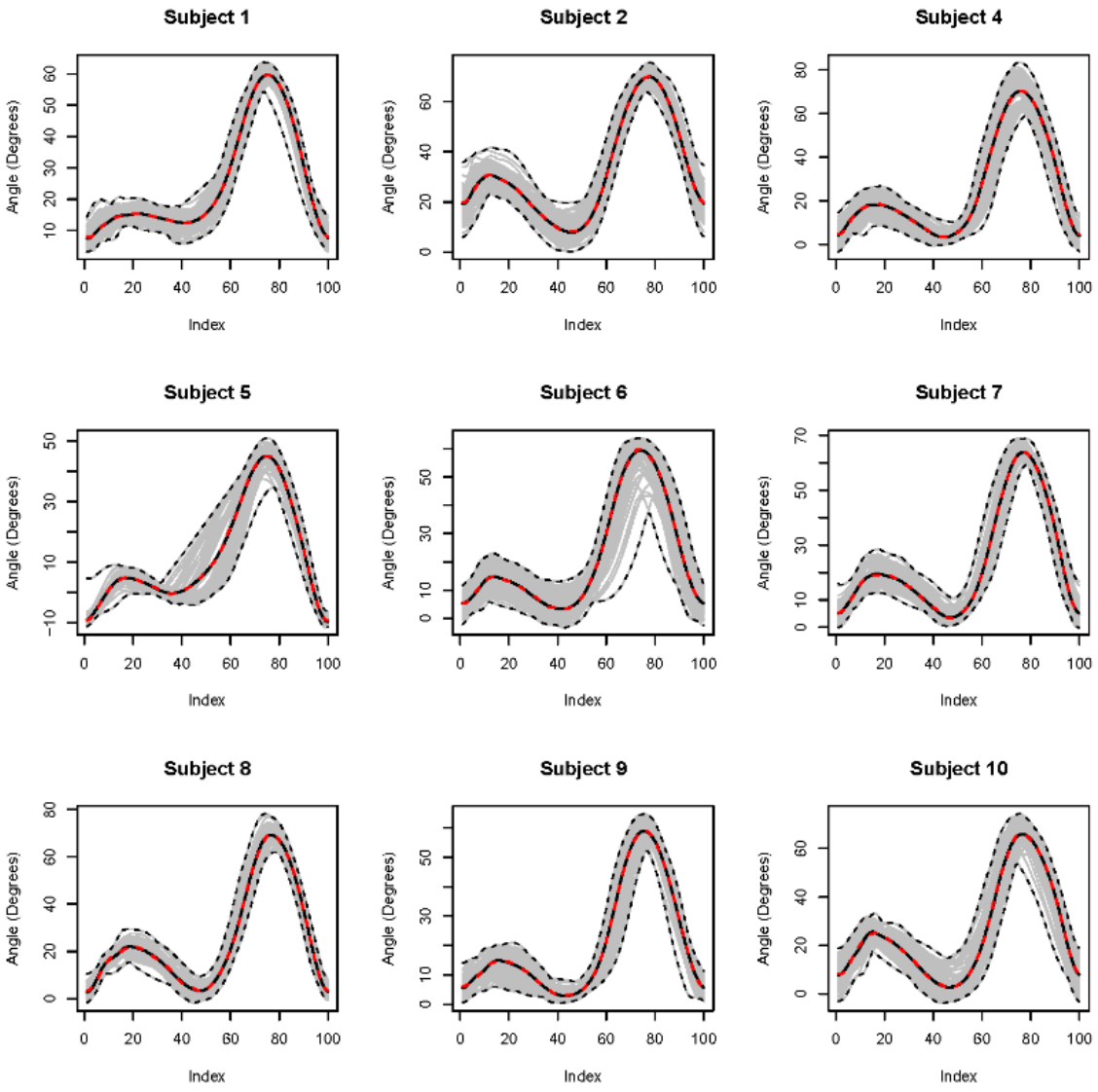

Figure 3-7: All stances for each subject are depicted in gray with the min and max stances in dotted gray. The average knee angles for all stances are depicted in black with the average prediction in dotted red.

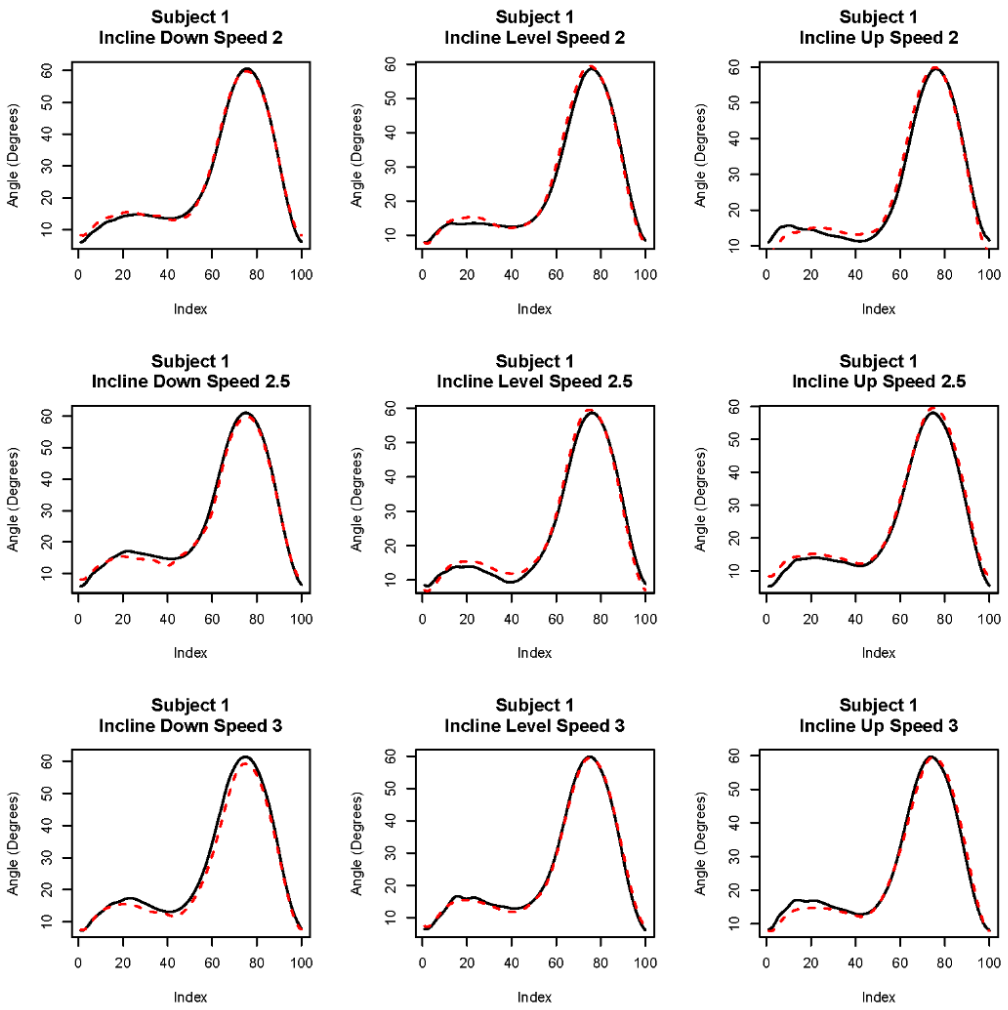

Figure 3-8: Average stride for each speed and incline for one subject.

Table 3-1: RMSE across speeds and inclines for the functional data model.

	Slow Speed [MPH]	Medium Speed [MPH]	Fast Speed [MPH]	Average [MPH]
Up	3.94	2.79	2.93	3.15
Level	3.48	3.03	3.16	3.16
Decline	3.54	2.85	3.50	3.31
Average	3.62	2.92	3.24	3.40

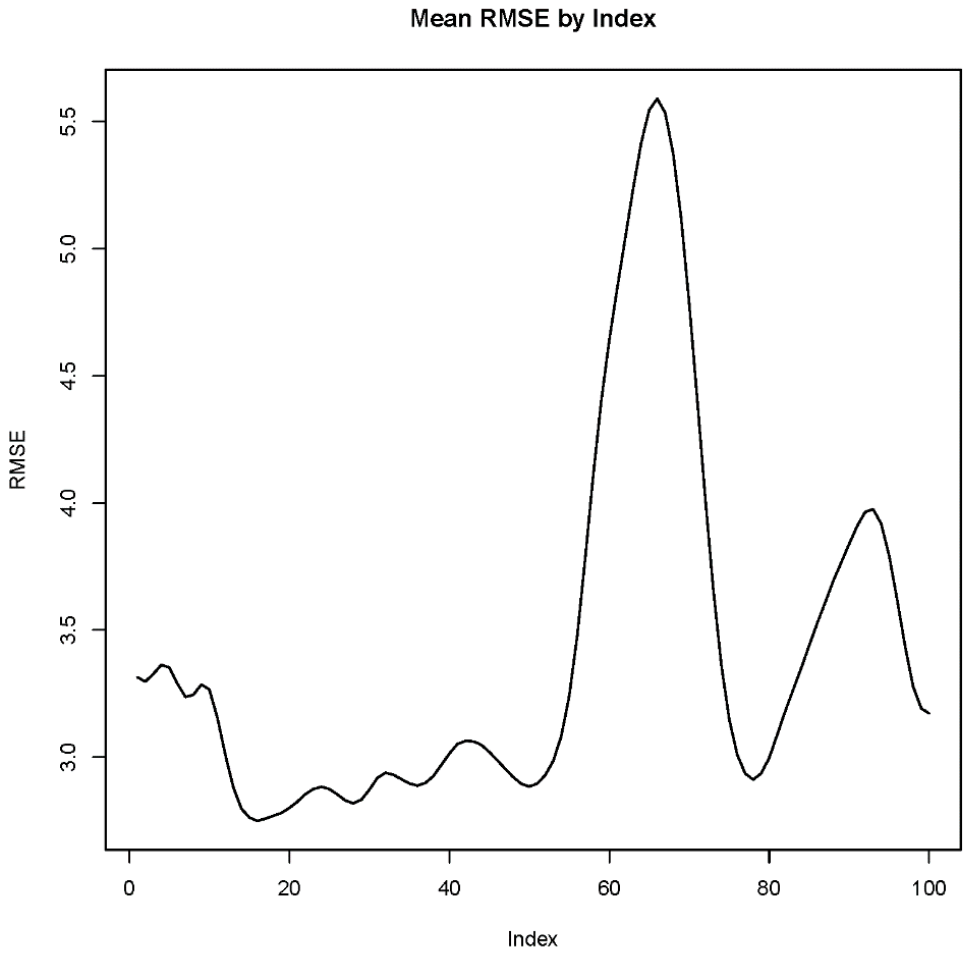

Figure 3-9: RMSE by index for all subjects.

3.4.3 Discrete linear regression model

The discrete linear regression model sacrificed overall accuracy in favor of highly accurate prediction of specific points (the inflection points) on the knee angle kinematics graph. The inflection points are more easily communicated and compared numerically between kinematic studies (as compared to the entire knee kinematics curve) and have been shown to contain highly useful patient diagnostic information [6, 13, 60]. The three inflection points of the

knee angle kinematics graph were defined by 2 discrete coordinates for each point: a knee angle magnitude and its corresponding time within the gait cycle (Figure 3-10): $t_{\text{max stance}}$, $\theta_{\text{max stance}}$, $t_{\text{midstance}}$, $\theta_{\text{midstance}}$, $t_{\text{max swing}}$, $\theta_{\text{max swing}}$.

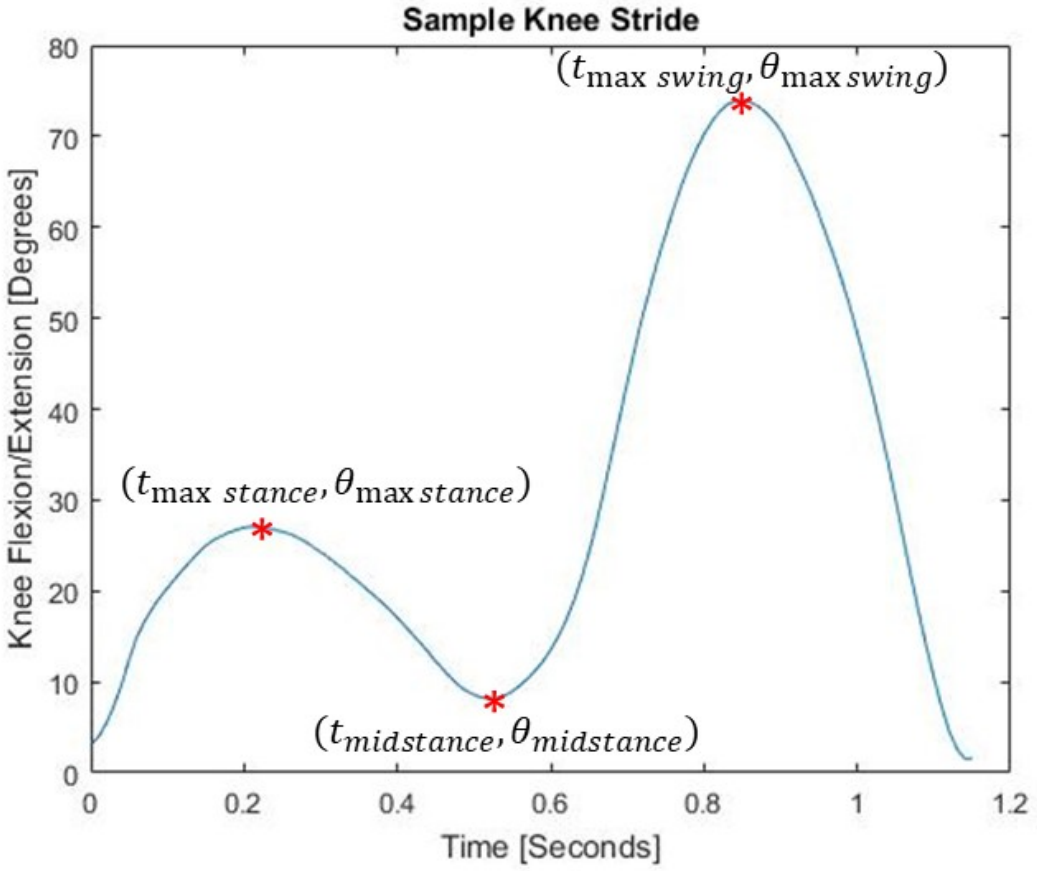

Figure 3-10: Discrete points estimated by linear regression model.

A separate model was created for each subject and 7 response variables derived from the sensor data were utilized in each model (3 voltage inflection points, 2 time values, a maximum derivative value, and the voltage at the max derivative value). A 10-fold cross validation procedure was carried out on the data for each distinct knee characteristic, which acted as the different response variables. The procedure found the model with the lowest cross validation

error. To evaluate the performance for each subject, the RMSE using the residuals from the final selected model was calculated across all six point coordinates. To assess performance in relation to the FDA model, the discrete linear regression model RMSE for each of the six point coordinates was compared to the RMSE of the FDA model at the same six points. All statistical analyses were conducted using R Statistical Software.

Overall, the RMSEs for all the discrete measures for the discrete linear regression model and FDA model are found in Table 3-2. On average, the RMSE for the three angle measures was 1.92° and for the three time measures the average was 0.0332 seconds. In every estimate of the six discrete measures, the discrete linear regression model performed better than the FDA model.

Table 3-2: RMSE of discrete linear regression model and FDA model for all six discrete points.

	Maximum Angle During Swing Phase [degrees]	Time to Maximum Angle During Swing Phase [seconds]	Local Maximum Angle During Stance Phase [degrees]	Time to Local Maximum Angle During Stance Phase [seconds]	Minimum Midstance Angle [degrees]	Time to Midstance Angle [seconds]
Discrete Linear Regression Model RMSE	1.7505	0.0129	1.7337	0.0300	2.2726	0.0284
FDA RMSE	2.693	0.0199	2.756	0.0412	2.886	0.0384

3.4.4 Machine learning models

A machine learning model was used to predict speed and categorical incline (3% downhill, level and 3% uphill) based on the same extracted response variables described in the

discrete linear regression model. A random forest machine learning approach was used to create the model based on 10-fold cross validation. For all models the bag size was 100, the number of iterations was 100, the minimum number of instances per leaf was one, an unlimited max depth of tree, and the desired batch size for batch prediction was 100. Two models were created for both speed and incline. The first used all 7 response variables from the discrete linear regression model. The second used a greedy stepwise process to pick the best response variables to be used in the random forest, without relying upon response variables that did not contribute significantly to model accuracy. The confusion matrix is reported below for the incline and the RMSE is reported for speed. All models and greedy stepwise processes were run using WEKA [61].

The confusion matrix for the full model (all 7 response variables) is found in Table 3-3. Overall, it correctly predicted the incline 90% of the time. For the second model (reduced parameter model), the greedy stepwise optimization process picked two predictors: voltage at the first max peak and minimum voltage preceding the first max peak. With this simplified 2-parameter model, it correctly classified the instances 82% of the time and its confusion matrix is also found in Table 3-3. For predicting speed, the full model had an RMSE of 0.23 MPH and its correlation coefficient was 0.952. For the reduced parameter model the greedy stepwise process identified three predictor variables: minimum voltage preceding the first max peak, the time to the same minimum, and the duration from that minimum to the stride's end time. This 3-parameter speed model's RMSE was 0.27 MPH and its correlation coefficient was 0.9337. It was noted that simplified models performed comparably well at predicting incline and speed when compared to the full models with only a few (2-3) predictors.

Table 3-3: Confusion matrix for machine learning treadmill incline prediction.

Model	Slope	Classified as 3 % Downhill	Classified as Level	Classified as 3 % Uphill	Sensitivity
All Discrete Predictors Included	3% Downhill	229	16	18	87.1%
	Level	12	422	32	90.6%
	3% Uphill	14	29	422	90.8%
	Precision	89.8%	90.4%	89.4%	90.1%
Simplified Greedy Stepwise Model	3% Downhill	200	26	37	76.0%
	Level	26	420	53	84.2%
	3% Uphill	28	47	390	83.9%
	Precision	85.5%	85.2%	81.3%	82.3%

3.5 Discussion

In previous work, Nakamoto et al., demonstrated the capability of measuring knee angles using a capacitive sensor under very controlled conditions (knee angles were virtually identical across all cycles) [25]. Our work demonstrates a step-forward in methodology and challenge, addressing knee angles that varied across trials due to changes in subject's speed and inclination. The angles measured varied from subject to subject and from trial to trial. This is similar to the work of Mengüç et. al. who used a liquid metal high deflection strain gauge embedded in an elastomer and measured three healthy males at multiple speeds including running speeds [29]. This work does not include running speeds or other joints as Mengüç et. al., but does include an older subject population (picked because of the possible applications in total knee replacements,

knee osteoarthritis, and Alzheimer's), more subjects (nine vs. three), and includes incline as a variable. This work also explores how to overcome a non-monotonic response, common in high deflection strain gauges, using advanced modeling techniques. Overall, the results demonstrate the ability of the wearable HDSG sensor system to estimate both discrete and continuous flexion/extension angles in the knee during walking gait, as well as estimate speed and incline.

The FDA model excelled at predicting continuous knee angles for the average stance of each subject overall and at each speed and incline (Figures 3-7 and 3-8). Though each subject had varying distributions of gait across all speeds, the model still performed well at estimating the average knee angle throughout the gait cycle. It also performed reasonably well at predicting knee angle within each individual stance, with the largest magnitude error occurring close to the transition between stance and swing phase. This could be due to the unloading of the leg which would cause an abrupt change in skin strain and in turn, the sensor estimated knee angle. Additional testing is needed to confirm this hypothesis. Errors for the FDA model were comparable to those found by Nakamoto et. al. (mean=4.4° standard deviation=3.6°) [25]; though the methodology of the present work utilized a more challenging nonlinear sensor and test conditions included walking gait and not just timed flexing of the knee. Mengüç et. al. reported higher errors for knee angle estimation compared to the present work with respect to all speeds. Their linear model does not include the average stance, which this work includes, and could benefit from more complex modeling techniques [29]. The error does not reach as low as 0.7° which was reported by some authors using IMUs [24]. These models assume that the knee is a pure hinge, which is an incomplete model, and the models that do not make this assumption have comparable error to the present work [24]. This study is limited however, that neither transition gait, nor running gait were measured, nor were extreme incline or decline. For the

present work, individual strides were manually identified for analysis based on motion capture angle data but could feasibly be done using computer algorithms and the sensor data. Currently, the sensor system requires initial calibration with a motion capture system for each individual subject in order to be used outside of the laboratory.

The results also demonstrate the ability of the wearable sensor system to accurately approximate discrete flexion/extension knee angles. For many of the time discrete characteristics, RMSE values approached the limits of the 100 Hz sampling frequency (0.01 s). While the FDA model has the advantage of a continuous estimate of knee angle data, which is a necessary pre-requisite to compute power and joint moment when coupled with force; the discrete model is more accurate at identifying the peaks and troughs of knee flexion and can be useful in applications such as a diagnostic tool for knee osteoarthritis [60], success of total knee replacements [13], and gait cadence in Alzheimer's patients [6].

The machine learning model demonstrated the ability of the sensor system to approximate the speed and incline of a subject during walking gait which could be used in caloric expenditure models. The initial machine-learning model included six discrete parameters based upon the voltage characteristics noted for each stride. However, this model was subsequently simplified using a greedy stepwise selection process that was able to identify a limited parameter model with comparable accuracy to using all of the discrete parameters. The accuracy of estimation of speed by the HDSG is comparable to IMUs (.224 MPH) [62], (.111 MPH) [63] and not as good as GPS (.050MPH) [64]. Yet, HDSGs are not limited to an open sky like GPS and detect additional data such as joint angles. A continuous parameter comparison to IMU slope estimation was not comparable because only one grade (both 3% incline and 3% decline) was tested in this experiment. However, Sabatini et. al. did report a RMSE of 1.52%

RMSE of grade estimation for IMU slope estimation [63]. Hall et. al. gave evidence that caloric expenditure models should include speed to be more precise [57]. Lester et. al. discussed that slope of surface is also important for caloric expenditure [58]. He includes that estimations of incline made by GPS are sometimes inadequate due to sudden jumps in altitude when subjects approach buildings. HDSGs also have the potential to help predict speed and incline that could be used in caloric expenditure models.

It should be noted that though this work and others use motion capture-computed joint angles as the "gold standard" for comparison, these angles have non-insignificant errors associated with soft tissue artifact and additional error associated with assuming the knee is a revolute or spherical joint. Reinschmidt et. al., quantified motion capture knee flexion/extension RMSE to be 2.1° when compared to intra-cortical bone pins [30]. Andersen et. al. also used intra-cortical bone pins to show that mean error estimates in flexion/extension angles increased 0.6°±0.6° by using a spherical joint model and 1.0°±1.2° for a revolute joint model [31]. Motion capture's aggregated error from soft tissue artifact and model inaccuracies shown by these authors is comparable to this work's error in the FDA and discrete linear models, and it is virtually impossible to identify which of them is closer to the "true joint angle" without using more invasive technique (i.e., bone pins, fluoroscopy). With the current accepted motion capture set up, evidence suggests accuracy of knee joint angles cannot exceed 2°-3° RMSE when measured by IR motion capture.

The HDSG sensor system had sufficient accuracy in the FDA, discrete linear regression, and machine learning models for the four main research audiences of motion capture: biomechanists, exercise scientists, physicians, and athletes. Biomechanists currently use motion capture to measure continuous human knee kinematics which has an accuracy of 2°-3° RMSE

for flexion/extension knee angles. The FDA model had an overall accuracy of 3.4° RMSE which is comparable to the motion capture angle error. Physicians and exercise scientists in general use discrete points on the knee flexion/extension curve measured by motion capture. For example, peak knee extension angle early after knee replacement surgery could predict abnormal gait patterns twelve months after the surgery [65]. Specifically, the difference between the two groups is 5.7°. The discrete linear regression model had a RMSE of 2.7° which is within the error of motion capture and lower than the difference between the two groups and therefore acceptable to exercise scientists and physicians. Finally, athletes and exercise scientists currently use IMUs for many measurements including speed and incline. As discussed previously, HDSG are comparable to these devices in terms of error when predicting speed and more information is needed in order to compare errors for predicting incline. This HDSG measurement system was shown to have acceptable accuracies to the main groups that use human kinematic data.

4 CONCLUSION AND FUTURE WORK

This thesis describes the application of nanocomposite high deflection strain gauges (HDSG) to measure knee kinematics using the non-monotonic portion of the strain resistance curve. Knee flexion/extension angles and sensor voltage were measured simultaneously using a motion capture system and microcontroller while nine subjects walked at three different speeds at three different inclines. Four different models were used to identify distinct aspects of knee kinematics during gait. The results gave evidence that a nanocomposite HDSG has the ability to estimate knee kinematics, speed, and incline in walking gait.

There are many advantages of using a HDSG sensor system to measure kinematics when compared to a traditional motion capture system. HDSG sensors excel at being a low-profile, non-intrusive in sensor mounting, and at times a low-cost sensor. The defining characteristic of HDSG sensors, when compared to motion capture kinematic analysis, is their ability to measure kinematics outside of a calibrated volume in a low-profile way. They are not unique in that space (for example, IMUs have some of the same advantages). However, competing body-mounted technologies (such as IMU's) are often more applicable to measuring rigid body kinematics such limb motion, since they do not and cannot account for the non-ideal nature of actual joints. Since HDSG sensors span the joint, they intrinsically include these non-ideal characteristics in their data collection.

The characteristics of HDSG sensors could allow for more parties to participate in kinematic analysis. As more researchers enter the kinematic analysis arena because of this lower bar to entry, more important findings about a wider range of testing conditions and populations can be studied. As HDSG sensors become a reliable and repeatable system, many observational studies such as the kinematics of everyday life, kinematics of high impact sports such as American football, and kinematics of long-distance sports such as cross-country skiing could be analyzed. These measurements are mostly impossible using a traditional motion capture system.

One challenge of using HDSG includes creating a universal calibration system for customizing the sensor's response to the subject's anatomy and sensor placement. The evidence in this work suggests that a universal intrasubject model is unlikely to be the preferred approach to processing HDSG sensor data. Challenges include individual differences in skin tissue around each joint and variation of sensor placement from trial to trial. Soft tissue artifacts are most likely varied on different joint anatomies and could affect the accuracy and effectiveness of a lower body gait analysis. Skin tissue on the knee for example, does not conform to muscle and bone tissue as tightly as the skin tissue around the ankle. Mengüç gives evidence towards this theory when he reported less angle RMSE on the ankle than the knee [29]. Further testing would be needed to prove this hypothesis. A similar methodology presented in the present work could be utilized for sensor placement on ankle, knees, and hips to validate a HDSG sensor in all degrees of freedom.

Thus, future work should include development of a simple, quick, and standardized calibration procedure that can be applied independent of a motion capture system. For example, calibration could include walking on a normal treadmill at several designated speeds and

inclines, bending the joint to specific angles, or using a phone video camera to extract kinematic data while the sensor is being used.

In order to have complete kinematics of the lower body, further work should be pursued in the effects of sensor placement on the ankle, hips, and other degrees of freedom on all joints including the knee. The main benefit of having all lower body joints with all degrees of freedom angles is the possibility of obtaining complete kinematic and kinetic data that can be used in biomechanical analysis, clinical diagnostics and therapy, and in sport performance applications. This could be especially powerful when joint kinematics information is coupled with force sensing technology like the wearable foam insoles described by Rosquist [66] that can capture ground reaction forces.

The optimization of nanocomposite HDSG fillers according to the application would also further kinematic analysis. The incredible ability of nanocomposite HDSG to change properties such as critical strain, elongation at break, and sensitivity based on filler ratio has not yet been fully explored; especially as it relates to applications in measuring human kinematics. Since every joint has different strains, range of motions, and tissue artifacts, a method for optimizing the gauge to each joint could effectively reduce error in measuring kinematics. This advancement would help optimize the overall mobile gait analysis system.

Additionally, full characterization of mechanical and electrical drift due to cyclic fatigue, strain-rate dependence, temperature, and humidity to be included in future models would help the sensor system to be more reliable and repeatable. Remington did some initial analysis on the properties of cyclic fatigue in HDSG sensors [53] but did not separate or quantify possible electrical drift due to permanent mechanical degradation (breaking of nanofillers), recoverable drift due to viscoelastic properties of silicone, recoverable drift due to sliding of nanofillers in the

matrix, and recoverable drift due to internal heating of the HDSG sensor. The sensors may also mechanically degrade due to breaking or sliding of nanofillers. It may also be possible that the log-normal response changes due to a strain-rate dependence. Viscoelastic polymers inherently are strain-rate dependent which may affect the electrical properties such as the strain resistance curve and most likely affect physical properties such as time to elastic strain recovery. All of this additional information can feed into a model to better account for electrical and mechanical drift.

In the future, three different types of models can be utilized to overcome the difficulties already mentioned of using HDSG in kinematic analysis: physics-based model, statistical model, and machine learning. In a physics-based model, all the phenomena that changes the sensor voltage described in the previous paragraph would have to be quantified as well as all their interactions between the phenomena (i.e. temperature, humidity, strain-rate dependence, etc.). This would be a challenging undertaking and would likely include a very large design of experiments approach. The model would have physical meaning, but calibration would be very challenging to implement. Though the model would help to better understand how the sensor works, it may not be a very practical model. A statistical based model would also require testing the sensor in many conditions (many activities e.g. running, jumping, etc., varying temperatures and humidity) and could work for the application where it was quantified. A statistical model could be useful if a specific activity under specific conditions needed to be quantified but the model could not accurately extend outside of a calibrated activity. Unlike the physics-based model the statistical model will most likely have very little physical meaning. Finally, a machine learning model would also have to be "trained" under many conditions but over time would "learn" the interactions between these conditions. Theoretically with a large enough data set, the model could also fully estimate angles in all conditions. This approach is likely to be the most

robust. The largest challenge for each of these three modeling approaches will be getting enough data to make the models expand to more activities and conditions.

In conclusion, this work provides evidence that nanocomposite HDSG provide a suitable solution to measuring knee kinematics. As further studies are pursued, this technology can be integrated with force sensing foam to create a mobile gait analysis system. This system would increase the reach of gait analysis studies by making it less cost prohibitive and expand the type of activities measured. In essence, it would become a new tool for gait measurement that would open new fields of research.

REFERENCES

[1]. Bouchrika, I., *A Survey of Using Biometrics for Smart Visual Surveillance: Gait Recognition*, in *Surveillance in Action*. 2018, Springer. p. 3-23.

[2]. Winter, D.A., et al., *Biomechanical walking pattern changes in the fit and healthy elderly.* Physical therapy, 1990. **70**(6): p. 340-347.

[3]. Shaw, K.E., et al., *The effects of shoe-worn insoles on gait biomechanics in people with knee osteoarthritis: a systematic review and meta-analysis.* Br J Sports Med, 2018. **52**(4): p. 238-253.

[4]. Abdulhay, E., et al., *Gait and tremor investigation using machine learning techniques for the diagnosis of Parkinson disease.* Future Generation Computer Systems, 2018. **83**: p. 366-373.

[5]. Starck, J. and A. Hilton, *Surface capture for performance-based animation.* IEEE computer graphics and applications, 2007. **27**(3).

[6]. Cedervall, Y., K. Halvorsen, and A.C. Åberg, *A longitudinal study of gait function and characteristics of gait disturbance in individuals with Alzheimer's disease.* Gait & posture, 2014. **39**(4): p. 1022-1027.

[7]. Barth, J., et al. *Biometric and mobile gait analysis for early diagnosis and therapy monitoring in Parkinson's disease*. in *2011 Annual International Conference of the IEEE Engineering in Medicine and Biology Society*. 2011. IEEE.

[8]. Weiss, R.J., et al., *Gait pattern in rheumatoid arthritis.* Gait & posture, 2008. **28**(2): p. 229-234.

[9]. Gage, J.R., *Gait analysis. An essential tool in the treatment of cerebral palsy.* Clinical orthopaedics and related research, 1993(288): p. 126-134.

[10]. Narayanan, U.G., *The role of gait analysis in the orthopaedic management of ambulatory cerebral palsy.* Current opinion in pediatrics, 2007. **19**(1): p. 38-43.

[11]. Sutherland, D.H., et al., *The pathomechanics of gait in Duchenne muscular dystrophy.* Developmental Medicine & Child Neurology, 1981. **23**(1): p. 3-22.

[12]. Martin, C.L., et al., *Gait and balance impairment in early multiple sclerosis in the absence of clinical disability.* Multiple Sclerosis Journal, 2006. **12**(5): p. 620-628.

[13]. Rahman, J., et al., *Gait assessment as a functional outcome measure in total knee arthroplasty: a cross-sectional study.* BMC musculoskeletal disorders, 2015. **16**(1): p. 66.

[14]. Chiu, L.Z., M.A. Bryanton, and A.N. Moolyk, *Proximal-to-distal sequencing in vertical jumping with and without arm swing.* The Journal of Strength & Conditioning Research, 2014. **28**(5): p. 1195-1202.

[15]. Huchez, A., et al., *Local versus global optimal sports techniques in a group of athletes.* Computer methods in biomechanics and biomedical engineering, 2015. **18**(8): p. 829-838.

[16]. Laughlin, W.A., et al., *The effects of baseball bat mass properties on swing mechanics, ground reaction forces, and swing timing.* Sports biomechanics, 2016. **15**(1): p. 36-47.

[17]. Brainerd, E.L., et al., *X-ray reconstruction of moving morphology (XROMM): precision, accuracy and applications in comparative biomechanics research.* Journal of Experimental Zoology Part A: Ecological Genetics and Physiology, 2010. **313**(5): p. 262-279.

[18]. Fuller, J., et al., *A comparison of lower-extremity skeletal kinematics measured using skin-and pin-mounted markers.* Human movement science, 1997. **16**(2-3): p. 219-242.

[19]. Maletsky, L.P., J. Sun, and N.A. Morton, *Accuracy of an optical active-marker system to track the relative motion of rigid bodies.* Journal of biomechanics, 2007. **40**(3): p. 682-685.

[20]. Peters, A., et al., *Quantification of soft tissue artifact in lower limb human motion analysis: a systematic review.* Gait & posture, 2010. **31**(1): p. 1-8.

[21]. Windolf, M., N. Götzen, and M. Morlock, *Systematic accuracy and precision analysis of video motion capturing systems—exemplified on the Vicon-460 system.* Journal of biomechanics, 2008. **41**(12): p. 2776-2780.

[22]. Schurr, S.A., et al., *Two-dimensional video analysis is comparable to 3d motion capture in lower extremity movement assessment.* International journal of sports physical therapy, 2017. **12**(2): p. 163.

[23]. Wong, C., et al., *Wearable Sensing for Solid Biomechanics: A Review.* Sensors Journal, IEEE, 2015. **15**(5): p. 2747-2760.

[24]. Picerno, P., *25 years of lower limb joint kinematics by using inertial and magnetic sensors: A review of methodological approaches.* Gait & Posture, 2017. **51**: p. 239-246.

[25]. Nakamoto, H., et al., *Joint angle measurement by stretchable strain sensor.* Journal of Ambient Intelligence and Humanized Computing, 2018: p. 1-6.

[26]. Cheng, Y., et al., *A Stretchable and Highly Sensitive Graphene-Based Fiber for Sensing Tensile Strain, Bending, and Torsion.* Advanced Materials, 2015. **27**(45): p. 7365-7371.

[27]. Yamada, T., et al., *A stretchable carbon nanotube strain sensor for human-motion detection.* Nature nanotechnology, 2011. **6**(5): p. 296-301.

[28]. Martineau, A., et al., *Skin Strain Measurement to Predict Knee Joint Angles through Nanocomposite Stain Gauges.* 2017.

[29]. Mengüç, Y., et al., *Wearable soft sensing suit for human gait measurement.* The International Journal of Robotics Research, 2014: p. 0278364914543793.

[30]. Reinschmidt, C., et al., *Tibiofemoral and tibiocalcaneal motion during walking: external vs. skeletal markers.* Gait & Posture, 1997. **6**(2): p. 98-109.

[31]. Andersen, M.S., et al., *Do kinematic models reduce the effects of soft tissue artefacts in skin marker-based motion analysis? An in vivo study of knee kinematics.* Journal of biomechanics, 2010. **43**(2): p. 268-273.

[32]. Amjadi, M., et al., *Stretchable, Skin-Mountable, and Wearable Strain Sensors and Their Potential Applications: A Review.* Advanced Functional Materials, 2016.

[33]. Bilodeau, R.A., et al., *Evolution of nano-junctions in piezoresistive nanostrand composites.* Composites Part B: Engineering, 2015. **72**: p. 45-52.

[34]. Johnson, O.K., et al., *The colossal piezoresistive effect in nickel nanostrand polymer composites and a quantum tunneling model.* Computers, Materials, & Continua, 2010. **15**(2): p. 87-112.

[35]. Johnson, O.K., et al., *Multiscale model for the extreme piezoresistivity in silicone/nickel nanostrand nanocomposites.* Metallurgical and Materials Transactions A, 2011. **42**(13): p. 3898-3906.

[36]. Baradoy, D.A., *Composition Based Modaling of Silicone Nano-Composite Strain Gauges.* 2015.

[37]. Johnson, O.K., et al., *Optimization of nickel nanocomposite for large strain sensing applications.* Sensors and Actuators A: Physical, 2011. **166**(1): p. 40-47.

[38]. Qian, Z., et al., *Inverse Piezoresistive Nanocomposite Sensors for Identifying Human Sitting Posture.* Sensors, 2018. **18**(6): p. 1745.

[39]. Hyatt, T., et al., *Nano-composite Sensors for Wide Range Measurement of Ligament Strain*, in *Experimental and Applied Mechanics, Volume 6*. 2011, Springer. p. 359-364.

[40]. Johnston, I., et al., *Mechanical characterization of bulk Sylgard 184 for microfluidics and microengineering.* Journal of Micromechanics and Microengineering, 2014. **24**(3): p. 035017.

[41]. Smooth-On. *Ecoflex™ 00-30*. [cited 2018 11-22]; Ecoflex 00-30 technical data]. Available from: https://www.smooth-on.com/products/ecoflex-00-30/.

[42]. Boland, C.S., et al., *Sensitive, high-strain, high-rate bodily motion sensors based on graphene–rubber composites.* ACS nano, 2014. **8**(9): p. 8819-8830.

[43]. Gong, S., et al., *Tattoolike polyaniline microparticle-doped gold nanowire patches as highly durable wearable sensors.* ACS applied materials & interfaces, 2015. **7**(35): p. 19700-19708.

[44]. Jeong, Y.R., et al., *Highly stretchable and sensitive strain sensors using fragmentized graphene foam.* Advanced Functional Materials, 2015. **25**(27): p. 4228-4236.

[45]. Kang, D., et al., *Ultrasensitive mechanical crack-based sensor inspired by the spider sensory system.* Nature, 2014. **516**(7530): p. 222.

[46]. Lu, N., et al., *Highly sensitive skin-mountable strain gauges based entirely on elastomers.* Advanced Functional Materials, 2012. **22**(19): p. 4044-4050.

[47]. Mattmann, C., F. Clemens, and G. Tröster, *Sensor for measuring strain in textile.* Sensors, 2008. **8**(6): p. 3719-3732.

[48]. Xiao, X., et al., *High-strain sensors based on ZnO nanowire/polystyrene hybridized flexible films.* Advanced materials, 2011. **23**(45): p. 5440-5444.

[49]. Amjadi, M., et al., *Highly stretchable and sensitive strain sensor based on silver nanowire–elastomer nanocomposite.* ACS nano, 2014. **8**(5): p. 5154-5163.

[50]. Hwang, B.-U., et al., *Transparent stretchable self-powered patchable sensor platform with ultrasensitive recognition of human activities.* ACS nano, 2015. **9**(9): p. 8801-8810.

[51]. Muth, J.T., et al., *Embedded 3D printing of strain sensors within highly stretchable elastomers.* Advanced Materials, 2014. **26**(36): p. 6307-6312.

[52]. Roh, E., et al., *Stretchable, transparent, ultrasensitive, and patchable strain sensor for human–machine interfaces comprising a nanohybrid of carbon nanotubes and conductive elastomers.* ACS nano, 2015. **9**(6): p. 6252-6261.

[53]. Remington, T.D., *Biomechanical Applications and Modeling of Quantum Nano-Composite Strain Gauges.* 2014.

[54]. Hirsch, A., et al., *Intrinsically Stretchable Biphasic (Solid–Liquid) Thin Metal Films.* Advanced Materials, 2016.

[55]. Park, J., et al., *Giant tunneling piezoresistance of composite elastomers with interlocked microdome arrays for ultrasensitive and multimodal electronic skins.* ACS nano, 2014. **8**(5): p. 4689-4697.

[56]. Wu, H., et al., *Fibrous strain sensor with ultra-sensitivity, wide sensing range, and large linearity for full-range detection of human motion.* Nanoscale, 2018. **10**(37): p. 17512-17519.

[57]. Hall, C., et al., *Energy expenditure of walking and running: comparison with prediction equations.* Medicine and science in sports and exercise, 2004. **36**: p. 2128-2134.

[58]. Lester, J., et al. *Validated caloric expenditure estimation using a single body-worn sensor*. in *Proceedings of the 11th international conference on Ubiquitous computing*. 2009. ACM.

[59]. Ramsay, J., G. Hooker, and S. Graves, *Functional data analysis with R and MATLAB*. 2009: Springer Science & Business Media.

[60]. Heiden, T.L., D.G. Lloyd, and T.R. Ackland, *Knee joint kinematics, kinetics and muscle co-contraction in knee osteoarthritis patient gait.* Clinical biomechanics, 2009. **24**(10): p. 833-841.

[61]. Holmes, G., A. Donkin, and I.H. Witten. *Weka: A machine learning workbench*. in *Intelligent Information Systems, 1994. Proceedings of the 1994 Second Australian and New Zealand Conference on*. 1994. IEEE.

[62]. Yuan, Q. and I.-M. Chen, *Localization and velocity tracking of human via 3 IMU sensors.* Sensors and Actuators A: Physical, 2014. **212**: p. 25-33.

[63]. Sabatini, A.M., et al., *Assessment of walking features from foot inertial sensing.* IEEE Transactions on biomedical engineering, 2005. **52**(3): p. 486-494.

[64]. Schutz, Y. and R. Herren, *Assessment of speed of human locomotion using a differential satellite global positioning system.* Medicine and Science in Sports and Exercise, 2000. **32**(3): p. 642-646.

[65]. Levinger, P., et al., *Knee biomechanics early after knee replacement surgery predict abnormal gait patterns 12 months postoperatively.* Journal of Orthopaedic Research, 2012. **30**(3): p. 371-376.

[66]. Rosquist, P.G., et al., *Estimation of 3D ground reaction force using nanocomposite piezo-responsive foam sensors during walking.* Annals of biomedical engineering, 2017. **45**(9): p. 2122-2134.

APENDICES

This section includes all of the appendices for this work. Appendix A includes the instructions for manufacturing high deflection strain gauges (HDSG). Appendix B describes the process of reusing a HDSG and attaching it to a new piece of athletic tape. Appendix C describes the process of attaching a HDSG to the knee. Appendix D enumerates the mechanical preconditioning the HDSG experiences before placing it on the athletic tape. Appendix E goes into detail about the electrical circuit and setup. Appendix F is a compendium of all the code used in this work. It includes the models used in Visual 3-D and data processing, the preprocessing of motion capture angles and sensor voltage in Matlab, and the optimization routine for fitting a log-normal curve to sensor voltage data.

APPENDIX A. MANUFACTURE OF NANOCOMPOSITE HDSG

1. Calculate the amount of Nickel Nanostrands (NINS), Nickel Coated Carbon Fiber(NCCF), silicone part A, silicone part B, and thinner to be placed in in the HDSG based upon the volume fraction of conductive particles desired.
2. Push the NINS and NCCF through the wire meshes in separate containers. It can be appropriate to use NINS that have been pushed through the wire mesh on a previous date but the NCCF need to be pushed through the mesh that day.
3. Measure the appropriate amount of strained NCCF into the metal tin and make sure to avoid clumping.
4. Measure the appropriate amount of strained Nins into a second metal tin.
5. Shake well bottle containing thinner. Pour the appropriate amount of thinner directly into a plastic cup that fits into the centrifugal mixer container. You can use a paper towel to soak up any accidental excess. Do not use paper cups because the silicone gets absorbed into them.
6. Shake well the container containing the A side of the Silicone. Measure out the appropriate amount of A into the plastic mixing cup containing the thinner. Mix well by hand with glass rod.
7. Pour the NCCF into the cup containing side A and thinner. Mix well by hand with a glass rod. (it mixes a lot better if the NCCF is done first)
8. Put into centrifugal mixer for 10 seconds at 2000 rpm throughout the gauge making process.

9. Pour a little less than half of the NINS into the cup containing side A, thinner, and the NCCF. Mix well by hand with a glass rod.
10. Put into mixing machine for 10 seconds.
11. Measure the appropriate amount of side B into plastic cup containing ingredients
12. Mix well by hand and place into centrifugal mixer for 10 seconds.
13. Pour the rest of the Nins into the cup containing side A, side B, thinner, and the NCCF. Mix well by hand with a glass rod.
14. Place into centrifugal mixer for 10 seconds.
15. Repeat step 14 two more times. The mixture should have the consistency of toothpaste for high filler concentrations. 60 second is the max the nanoparticles can handle in the mixing machine before they start breaking down.
16. Spread the uncured gauge evenly onto the female portion of the mold using metal spatula making sure that it is pressed down into the edges and corners. The gauge material should be level throughout.

Vacuum

1. Place female portion of mold into vacuum
2. Put on lid to vacuum
3. Make sure the release valve on the pump and the cap is screwed into place
4. Turn on vacuum pump
5. When pressure gauge on top left is at 20psi turn knob so that it is vertical
6. Turn off pump
7. Wait 5 min
8. Turn the release valve horizontal and screw off cap to release air

9. When pressure gauge shows zero pressure open lid.
10. Smooth out gauge with metal spatula
11. Place male portion of mold onto female portion.
12. Press side to side and back to front to squeeze out any air bubbles.
13. Tighten down c-clamps one on each side of the mold to squeeze out any excess

Curing

1. Let it cure at room temperature for twenty-four hours
2. Alternatively, cure at room temperature for four hours
3. Turn on oven and set temperature at 80° Celsius
4. Put mold in oven and let it sit in oven for two hours at 80° C
5. Change temperature to 100° C and let sit for one hour
6. Turn off oven and using pliers take out mold and place on cardboard
7. When cool open mold using screwdriver
8. Using the knife cut along all edges Use flathead screwdriver gently lift gauge from bottom of mold

APPENDIX B. ATTACHING HDSG ONTO NEW PIECE OF ATHLETIC TAPE

1. After a HDSG attached to athletic tape has been used slowly remove the HDSG with the associated electrical components from the athletic tape.
2. Cut with scissors or a knife any excess clear silicone from sides of the strain gauge.
3. Cut new piece of athletic tape to correct size.
4. Put super glue on metal contacts of the electrical assembly and fasten to the athletic tape and let dry.
5. Using silicone glue reattach the rest of the HDSG to the athletic tape making sure that all parts of the HDSG attach to the athletic tape without putting any glue on the bottom of the HDSG.

APPENDIX C. ATTACHING STRAIN GAUGE TO KNEE

1. After subject has signed the necessary paperwork, have subject sit on flat stool and lay right leg on another flat stool of the same height.
2. Apply pre-spray adhesive according to manufacturer's instructions on the anterior parts of the right knee including three inches proximally and distally.
3. Remove backing of the athletic tape with the strain gauge attached and place the sensor centered on the axis of rotation of the knee. Be sure to press the tape to the contours of the knee
4. Clip in the sensor into the electrical circuit being sure that the gauge is connected to ground and that if an outside alternating current supply is used both the middle of the voltage divider and the ground are both measured.

APPENDIX D. HDSG PRECONDITIONING

Mechanical HDSG Preconditioning

1. Using a sharp exacto knife and a ruler, cut strain gauges into 6mm strips
2. Clamp the HDSG into the serrated grips for the mini-instron.
3. Measure length between grips and calculate 50% strain and stretch once using the manual settings on the instron.
4. Let gauge relax to recover its length
5. Repeat steps 3-4 until the differences between the length before and after stretching is within 1 mm.
6. Cut the portion of the sensor that was clamped by the serrated grips

APPENDIX E. ELECTRICAL CIRCUIT SET-UP

1. Fig 4-1 contains the schematic for the electrical circuit for sensing the gauge. V_{in} is an alternating current 3.2 V, all positive square wave. If the AC signal comes from the microcontroller sensing the V_{out1} then V_{out2} does not need to be measured. V_{out2} is measured and subtracted from V_{out1} in other cases to establish a common ground.

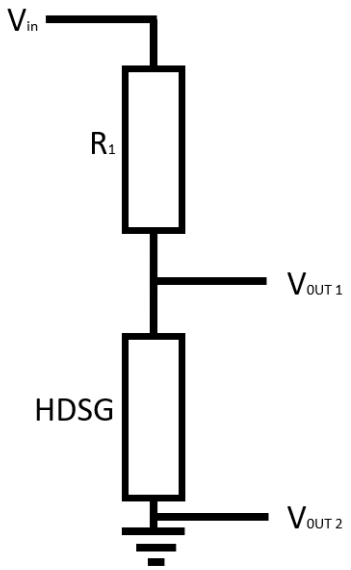

Figure 4-0-1 Electrical circuit of HDSG in voltage divider

2. The value of R_1 should be as close as possible to the value of the HDSG. It useful to have R_1 be a potentiometer to account for signal drift that occurs with increasing cycles in the sensor.
3. To connect the HDSG to wire use bare female disconnects. Be sure to solder wire onto disconnects before inserting sensor.
4. Use needle-nose pliers to pry open the crimped portion and insert sensor.
5. Place thick paper between the sensor and the metal flaps to protect the sensor from being cut.
6. Use pliers to crimp metal flaps onto the sensor

APPENDIX F CODE

Extracting angles from Vicon data using Visual 3D:

```
Create_Hybrid_Model
/CALIBRATION_FILE=
! /SUFFIX=
! /RANGE=ALL_FRAMES
/SET_PROMPT=Open standing file
;

Apply_Model_Template
/CALIBRATION_FILE=
/MODEL_TEMPLATE=C:\Users\Adin\Documents\fall 2016\BB C3Ds
/SET_PROMPT=Open model file
! /VIEW_BUILDMODEL_RESULTS=2
;

Set_Subject_Height
! /CALIBRATION_FILE=
! /HEIGHT=
! /UNITS=m
;

Set_Subject_Mass
! /CALIBRATION_FILE=
! /WEIGHT=
! /UNITS=Kg
;
```

```
!chosing movement files
File_Open
! /FILE_NAME=
! /SUFFIX=
/SET_PROMPT=Movement files
! /FILTER=
;

Assign_Model_File
! /CALIBRATION_FILE=
/MOTION_FILE_NAMES=ALL_FILES
! /REMOVE_EXISTING_ASSIGNMENTS=FALSE
;

!assigns tag to apply to certain files in the select active file function, can be applied more broadly
Assign_Tags_To_Files
/MOTION_FILE_NAMES=*run
! /QUERY=
/TAGS=run
;

!assigns tag to apply to certain files in the select active file function, can be applied more broadly
Assign_Tags_To_Files
/MOTION_FILE_NAMES=*walk
! /QUERY=
/TAGS=walk
;

Select_Active_File
/FILE_NAME=ALL_FILES
```

```
! /QUERY=
;

!GAP FILLER
Interpolate
/SIGNAL_TYPES=TARGET
! /SIGNAL_FOLDER=ORIGINAL
! /SIGNAL_NAMES=
! /RESULT_FOLDER=PROCESSED
! /RESULT_SUFFIX=
! /MAXIMUM_GAP=10
! /NUM_FIT=3
! /POLYNOMIAL_ORDER=3
;

Lowpass_Filter
/SIGNAL_TYPES=TARGET
/SIGNAL_FOLDER=PROCESSED
! /SIGNAL_NAMES=
! /RESULT_FOLDER=PROCESSED
! /RESULT_SUFFIX=
! /FILTER_CLASS=BUTTERWORTH
! /FREQUENCY_CUTOFF=6.0
! /NUM_REFLECTED=6
! /NUM_EXTRAPOLATED=0
! /TOTAL_BUFFER_SIZE=6
! /NUM_BIDIRECTIONAL_PASSES=1
;

Compute_Model_Based_Data
/RESULT_NAME=ang
```

/FUNCTION=JOINT_ANGLE

/SEGMENT=RShank

/REFERENCE_SEGMENT=RThigh

/RESOLUTION_COORDINATE_SYSTEM=

! /USE_CARDAN_SEQUENCE=FALSE

! /NORMALIZATION=FALSE

! /NORMALIZATION_METHOD=

! /NORMALIZATION_METRIC=

! /NEGATEX=FALSE

! /NEGATEY=FALSE

! /NEGATEZ=FALSE

! /AXIS1=X

! /AXIS2=Y

! /AXIS3=Z

! /TREADMILL_DATA=FALSE

! /TREADMILL_DIRECTION=UNIT_VECTOR(0,1,0)

! /TREADMILL_SPEED=0.0

;

Export_Data_To_Matfile

/SIGNAL_TYPES=LINK_MODEL_BASED

/SIGNAL_FOLDER=ORIGINAL

/SIGNAL_NAMES=ang

/FILE_NAME=c:\users\adin\documents\research\strain vs. motion capture\healthy\subject 5\ang.mat

/MATLAB_NAMES=ang

! /PARAMETER_NAMES=

! /PARAMETER_GROUPS=

! /OUTPUT_PARAMETER_NAMES=

/USE_NAN_FOR_DATANOTFOUND=TRUE

;

Model file for Visual 3D

!

! Model File Generated by Visual3D ModelBuilder

!

!

! Method For Computing Model Pose

!

!

! Model Pose Pipeline

!

!

! Model Metric Values

!

Set_Model_Metric

! /CALIBRATION_FILE=

/METRIC_NAME=Mass

/METRIC_VALUE=1

;

Set_Model_Metric

! /CALIBRATION_FILE=

/METRIC_NAME=Height

/METRIC_VALUE=1

;

Set_Model_Metric

! /CALIBRATION_FILE=

/METRIC_NAME=Gravity

/METRIC_VALUE=9.81

;

Set_Model_Metric

! /CALIBRATION_FILE=

/METRIC_NAME=Segment_to_COFP_Distance

/METRIC_VALUE=0.2

;

Set_Model_Metric

! /CALIBRATION_FILE=

/METRIC_NAME=Joint_Radius_Ratio

/METRIC_VALUE=1.1

;

Set_Model_Metric

! /CALIBRATION_FILE=

/METRIC_NAME=RThigh_Distal_Radius

/METRIC_VALUE=.1

;

Set_Model_Metric

! /CALIBRATION_FILE=

/METRIC_NAME=RShank_Distal_Radius

/METRIC_VALUE=.1

;

!

! Segment Info

!

! Segment RThigh

!

HYBRID_SEGMENT

! /CALIBRATION_FILE=

/TYPE=Visual_3D

/NAME=RThigh

/REFERENCE_OBJECT=Lateral Proximal+Proximal Joint+Distal Joint+Additional Object+Additional Plane+Distal Radius+Proximal Radius

/REFERENCE_OBJECT_NAMES=TSide+TLR+TDown+++RThigh_Distal_Radius+RThigh_Proximal_Radius

/REFERENCE_OBJECT_TYPES=LANDMARK+TARGET+LANDMARK+++METRIC+METRIC

/USE_CAL_TARGETS_FOR_TRACKING=FALSE
/TRACKING_TYPES=TARGET+TARGET+TARGET
/TRACKING_NAMES=TLR+TUL+TUR
! /USE_OPTIMAL_TRACKING=TRUE
! /DO_NOT_USE_LOCAL_TRANSFORMATION=FALSE
/KINEMATIC_ONLY=TRUE
! /STATIC_SEGMENT=FALSE
/GRAPHICS_ROT_X=0
/GRAPHICS_ROT_Y=0
/GRAPHICS_ROT_Z=0
/GRAPHICS_SCALE_X=1
/GRAPHICS_SCALE_Y=1
/GRAPHICS_SCALE_Z=1
/GRAPHICS_TRANSLATE_X=0
/GRAPHICS_TRANSLATE_Y=0
/GRAPHICS_TRANSLATE_Z=0
! /GRAPHICS_UNIT_SCALE=1.000000
! /GRAPHICS_SCALE_TO_SEG_LENGTH=TRUE
! /MASS=
/GEOMETRY=CONE
/PROX_TO_CG_AXIAL=0.5*RThigh_SEG_LENGTH
/PROX_TO_CG_ML=0*RThigh_SEG_LENGTH
/PROX_TO_CG_AP=0*RThigh_SEG_LENGTH
/IXX=-3333.33
/IYY=-3333.33
/IZZ=-5000
! /AP_DIRECTION=
! /AXIAL_DIRECTION=
/OBJFILE=rthigh.v3g
! /COLFILE=
! /DEPTH=

;

!

! Segment RShank

!

HYBRID_SEGMENT

! /CALIBRATION_FILE=

/TYPE=Visual_3D

/NAME=RShank

/REFERENCE_OBJECT=Proximal Joint+Lateral Proximal+Distal Joint+Additional Object+Additional Plane+Distal Radius+Proximal Radius

/REFERENCE_OBJECT_NAMES=SLR+SSide+SDown+++RShank_Distal_Radius+RShank_Proximal_Radius

/REFERENCE_OBJECT_TYPES=TARGET+LANDMARK+LANDMARK+++METRIC+METRIC

/USE_CAL_TARGETS_FOR_TRACKING=FALSE

/TRACKING_TYPES=TARGET+TARGET+TARGET

/TRACKING_NAMES=SLL+SLR+SUL

! /USE_OPTIMAL_TRACKING=TRUE

! /DO_NOT_USE_LOCAL_TRANSFORMATION=FALSE

/KINEMATIC_ONLY=TRUE

! /STATIC_SEGMENT=FALSE

/GRAPHICS_ROT_X=0

/GRAPHICS_ROT_Y=0

/GRAPHICS_ROT_Z=0

/GRAPHICS_SCALE_X=1

/GRAPHICS_SCALE_Y=1

/GRAPHICS_SCALE_Z=1

/GRAPHICS_TRANSLATE_X=0

/GRAPHICS_TRANSLATE_Y=0

/GRAPHICS_TRANSLATE_Z=0

! /GRAPHICS_UNIT_SCALE=1.000000

```
! /GRAPHICS_SCALE_TO_SEG_LENGTH=TRUE
! /MASS=
! /GEOMETRY=
/PROX_TO_CG_AXIAL=0.5*RShank_SEG_LENGTH
/PROX_TO_CG_ML=0*RShank_SEG_LENGTH
/PROX_TO_CG_AP=0*RShank_SEG_LENGTH
! /IXX=
! /IYY=
! /IZZ=
! /AP_DIRECTION=
! /AXIAL_DIRECTION=
! /OBJFILE=
! /COLFILE=
! /DEPTH=
;

!
! Digitizing Wand Configuration
!
HYBRID_DIGITIZING_WAND
! /CALIBRATION_FILE=
/WAND_ORIENTATION_MARKER1=
/WAND_ORIENTATION_MARKER2=
! /WAND_ORIENTATION_MARKER3=
! /OFFSET_X=0
! /OFFSET_Y=0
/OFFSET_Z=-0.127
! /OFFSET_X2=0
! /OFFSET_Y2=0
! /OFFSET_Z2=0
! /WAND_HAS_SPRING=TRUE
```

```
! /WAND_TRIGGER_MARKER1=
! /WAND_TRIGGER_MARKER2=
! /WAND_TRACKING_MARKERS=
;
!
! Landmarks
Add_Landmark
/LANDMARK_NAME=TDown
! /CALIBRATION_FILE=
! /USER_GENERATED=TRUE
! /USE_PERCENTAGE=FALSE
/CALIBRATION_ONLY=TRUE
! /USE_TARGETS=FALSE
/SEGMENT_NAME=LAB
/TARGET_TYPES=TARGET
/TARGET_NAMES=TLR
! /MCS_ML=0.0
! /MCS_AP=0.0
/MCS_AXIAL=-0.1
! /LANDMARK_LOCATION=
! /REFERENCE_LOCATION_TYPE=
! /REFERENCE_LOCATION_NAME=
! /USE_REFERENCE_LOCATION=FALSE
;
Add_Landmark
/LANDMARK_NAME=TSide
! /CALIBRATION_FILE=
! /USER_GENERATED=TRUE
! /USE_PERCENTAGE=FALSE
/CALIBRATION_ONLY=TRUE
! /USE_TARGETS=FALSE
```

```
/SEGMENT_NAME=LAB
/TARGET_TYPES=TARGET
/TARGET_NAMES=TLR
! /MCS_ML=0.0
/MCS_AP=-0.1
! /MCS_AXIAL=0.0
! /LANDMARK_LOCATION=
! /REFERENCE_LOCATION_TYPE=
! /REFERENCE_LOCATION_NAME=
! /USE_REFERENCE_LOCATION=FALSE
;
Add_Landmark
/LANDMARK_NAME=SDown
! /CALIBRATION_FILE=
! /USER_GENERATED=TRUE
! /USE_PERCENTAGE=FALSE
/CALIBRATION_ONLY=TRUE
! /USE_TARGETS=FALSE
/SEGMENT_NAME=LAB
/TARGET_TYPES=TARGET
/TARGET_NAMES=SLR
! /MCS_ML=0.0
! /MCS_AP=0.0
/MCS_AXIAL=-.1
! /LANDMARK_LOCATION=
! /REFERENCE_LOCATION_TYPE=
! /REFERENCE_LOCATION_NAME=
! /USE_REFERENCE_LOCATION=FALSE
;
Add_Landmark
/LANDMARK_NAME=SSide
```

```
! /CALIBRATION_FILE=
! /USER_GENERATED=TRUE
! /USE_PERCENTAGE=FALSE
! /CALIBRATION_ONLY=FALSE
! /USE_TARGETS=FALSE
/SEGMENT_NAME=LAB
/TARGET_TYPES=TARGET
/TARGET_NAMES=SLR
! /MCS_ML=0.0
/MCS_AP=-.1
! /MCS_AXIAL=0.0
! /LANDMARK_LOCATION=
! /REFERENCE_LOCATION_TYPE=
! /REFERENCE_LOCATION_NAME=
! /USE_REFERENCE_LOCATION=FALSE
;
!
! Muscles
!
```

```
Convert Strain Gauge Files into Usable Format for Matlab
clear all

files=dir('*.csv');     %find all file names I want

for i=1:length(files)
   name=files(i).name;     %names of all the files
    varname=regexp(name,'._(\d\w*).csv','tokens'); %extract the end part of the file as a variable
name
   varname=char(varname{1} );    %turn into a string
   varname=strcat('g',varname);
```

```
    eval([varname '=csvread(name,1,5);'])
    eval([varname '=' varname '(:,2)-' varname '(:,1);'])
end

clear files
clear i
clear name
clear varname
clear x

save strain

Save Vicon Files into useable format for Matlab
load ang.mat

for i=1:length(FILE_NAME)
    name=FILE_NAME{i,1};     %names of all the files
    varname=regexp(name,'Vicon\\(\d\w*).c3d','tokens'); %extract the end part of the file as a
variable name
    varname=char(varname{1});    %turn into a string
    varname=strcat('v',varname);
    eval([varname '='  'ang{i,1};'])
    eval([varname '='  '-' varname '(:,1);'])
end

clear ANALOG_VIDEO_FRAME_RATIO
clear ang
clear FILE_NAME
clear FRAME_RATE
clear i
clear name
```

```
clear varname

save ang
```

Main matlab code for lining up data

```
%Subject 8 data
clear all
close all

% sdata
load strain
load ang

%2MPH down
[S2mphD,V2mphD,t2mphD]=datfix(g2down,v2mphdownhill);
M2mphD=[S2mphD,V2mphD,t2mphD];
xlswrite('2MPH down',M2mphD)

%2mph uphill
[S2mphU,V2mphU,t2mphU]=datfix(g2up,v2mphuphill);
M2mphU=[S2mphU,V2mphU,t2mphU];
xlswrite('2MPH uphill',M2mphU)


%2mph level
[S2mphL,V2mphL,t2mphL]=datfix(g2level,v2mphlevel);
M2mphL=[S2mphL,V2mphL,t2mphL];
xlswrite('2MPH level',M2mphL)

%3MPH down
[S3mphD,V3mphD,t3mphD]=datfix(g3down,v3mphdownhill);
```

```
M3mphD=[S3mphD,V3mphD,t3mphD];
xlswrite('3MPH down',M3mphD)

%3mph uphill
[S3mphU,V3mphU,t3mphU]=datfix(g3up,v3mphuphill);
M3mphU=[S3mphU,V3mphU,t3mphU];
xlswrite('3MPH uphill',M3mphU)

%3mph level
[S3mphL,V3mphL,t3mphL]=datfix(g3level,v3mphlevel);
M3mphL=[S3mphL,V3mphL,t3mphL];
xlswrite('3MPH level',M3mphL)

%4mph uphill
[S4mphU,V4mphU,t4mphU]=datfix(g4up,v4mphuphill);
M4mphU=[S4mphU,V4mphU,t4mphU];
xlswrite('4MPH uphill',M4mphU)

%4mph level
[S4mphL,V4mphL,t4mphL]=datfix(g4level,v4mphlevel);
M4mphL=[S4mphL,V4mphL,t4mphL];
xlswrite('4MPH level',M4mphL)

%4mph down
[S4mphD,V4mphD,t4mphD]=datfix(g4down,v4mphdownhill);
M4mphD=[S4mphD,V4mphD,t4mphD];
xlswrite('4MPH down',M4mphD)
```

Matlab function within “main.m” to line up data sets

```
function [sfin,vfin,t]=datfix(svec,vvec)
```

```
%frequencies of the AC signal and microcontroller
AC=100;
micro=1031;
vicon=100;

%filter variables
cut=2;  %cut off frequency
Wn=cut*2*.8*pi/AC;  %normalized sampling frequency
[b,a]=butter(4,Wn); %low pass filter coefficients

%Strain vector
svec=rmser(AC,micro,svec);      %Change from AC to DC and also does a 100 hz low pass filter
svec=filtfilt(b,a,svec);        %low pass filter

%vicon
vvec=resample(vvec,AC,vicon);   %make the vectors the same sampling frequencies

%plot and check starting point
figure
yyaxis right
plot(vvec)
yyaxis left
plot(svec)
legend('SG','Vicon')

%lining up the vectors
bi=input('Is the strain data ahead of vicon? [1/0]');
diff=input('What is difference between starting points?');

%lining up start points
if bi==0 && diff==0
```

```
    svec=svec(1:end);
    vvec=vvec(1:end);
elseif bi==1 && diff>0
    svec=svec(diff:end);
else
    vvec=vvec(diff:end);
end

%making them the same size
if length(svec)>length(vvec)
    sfin=svec(1:length(vvec));
    vfin=vvec;
else
    vfin=vvec(1:length(svec));
    sfin=svec;
end
t=0:1/AC:(length(vfin)-1)/AC;
t=t';

figure
yyaxis right
plot(t,vfin)
ylabel('Angle [deg]')
yyaxis left
plot(t,sfin)
ylabel('Voltage [V]')
title('Strain Gauge vs Vicon')
end
```

Function within “main.m” to turn the AC sensor signal into a DC signal

```
function rmsed=rmser(ACfreq,SAMPLEfreq,vector)
```

```
vector=resample(vector,1000,SAMPLEfreq);

sec=floor(1000/ACfreq);

rmsed=zeros(floor(length(vector)/sec),1);

for i=1:floor(length(vector)/sec)

   rmsed(i)=rms(vector(i*sec-(sec-1):sec*i));

end
```

Matlab code for lognormal fitting

```
clear all


load alldivsubs_woNaN

ang8=ang8+15;

fo=fitoptions('Method','NonlinearLeastSquares','Display','iter','Robust','Bisquare','Lower',...
   [1e-10 1e-10 1e-10],'Upper',[1e100 1e100 1e100],'StartPoint',[.95 90 .35]);

%  opts.MaxFunEvals=1000;
% opts.DiffMaxChange=.1;

g=fittype('d.*(1./(a.*((ang)./c).*sqrt(2.*pi)).*exp(-((log((ang)./c)).^2)./(2.*a.^2)))',...
   'independent','ang', 'dependent','volt','coefficients',{'a' 'c' 'd'},'options',fo);


[myfit,G]=fit(ang8',volt8,g)
plot(myfit,ang8,volt8)
```